Technical Meeting on A Database of Atomic Configuration Formed in Collision Cascades

The analytic embedded atom method and its application to computer simulations for radiation damage

Wangyu Hu

Hunan University, Changsha 410082, China

2017.11.16

Outline of the report

1， Modified analytic embedded-atom method (MAEAM)

2， Irradiation damage in helium doping iron

3，Irradiation damage in NiMo binary alloy

4， Irradiation damage in helium doping vanadium

5， Irradiation damage in tungsten

6， Irradiation damage in amorphous

7, Fe(001)-Li solid-liquid interface under irradiation

modified analytic embedded-atom method

For pure elements

Modified analytic embedded atom method (MAEAM)

$$E_{tot} = \sum_i E_i \quad (1) \qquad E_i = \frac{1}{2}\sum_{j\neq i}\phi(r_{ij}) + F(\rho_i) + M(P_i) \quad (2)$$

Pair body potential

$$\varphi(r) = \begin{cases} k_0 + k_1\left(\frac{r}{r_1}\right) + k_2\left(\frac{r}{r_1}\right)^2 + k_3\left(\frac{r}{r_1}\right)^3 + k_4\left(\frac{r_1}{r}\right) & r \le r_e \\ \left[k_5\left(\frac{r}{r_1}\right)^2 + k_6\left(\frac{r}{r_1}\right)^4 + k_7\left(\frac{r_1}{r}\right)^6\right](1-\frac{r}{r_c})^2 & r_e \le r \le r_c \end{cases} \quad (3)$$

Embedding energy

$$F(\rho_i) = -f_0[1 - n\ln(\frac{\rho_i}{\rho_e})](\frac{\rho_i}{\rho_e})^n \quad (4) \qquad \rho_i = \sum_{j\neq i} f_e(\frac{r_1}{r_{ij}})^{\beta}(\frac{r_{ce}-r_{ij}}{r_{ce}-r_1})^2 \quad (5)$$

modified analytic embedded-atom method

Modified energy

$$M(P_i) = \alpha[1\text{-}\cos(10\pi \frac{P_i - P_e}{P_e})] \quad (6)$$

$$P_i = \sum_{j \neq i} g_e (\frac{r_1}{r_{ij}})^{\gamma} (\frac{r_{ce} - r_{ij}}{r_{ce} - r_1})^2 \quad (7)$$

Cross interaction term

$$\phi^{ab}(r_{ij}) = \frac{1}{2}\mu[\phi^a(r_{ij}\frac{r^a}{r^c}) + \phi^b(r_{ij}\frac{r^b}{r^c})] \quad (8)$$

The parameters in the cross interaction term obtained by fitting the formation enthalpy of Ni-Mo alloys

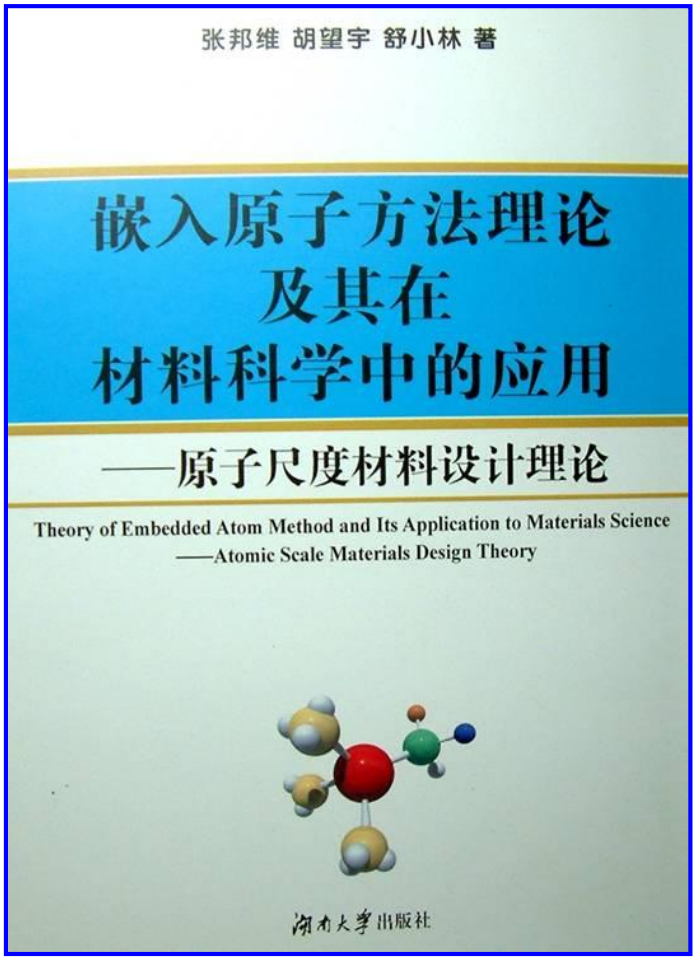

Backgrounds

Reduced activation materials for fusion reactor

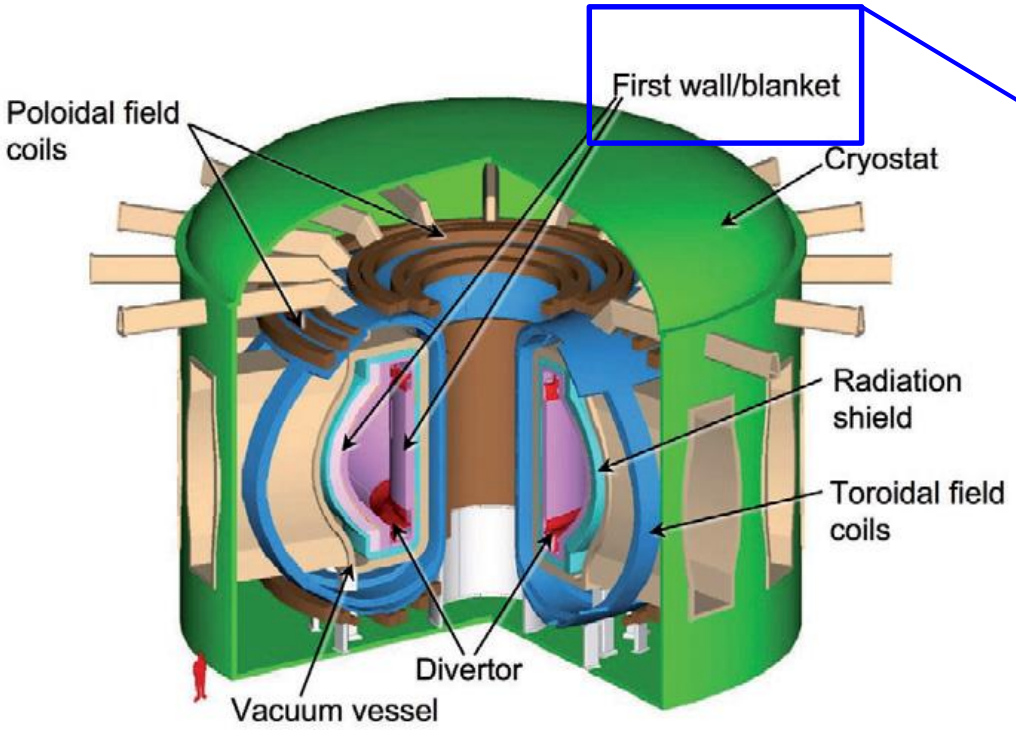

- Reduced activation ferritic/martensitic (RAFM) steel ;
- Vanadium based alloys (V-4Ti-4Cr/V-5Ti-5Cr);
- SiC_f/SiC composites

Clustering properties of helium in iron

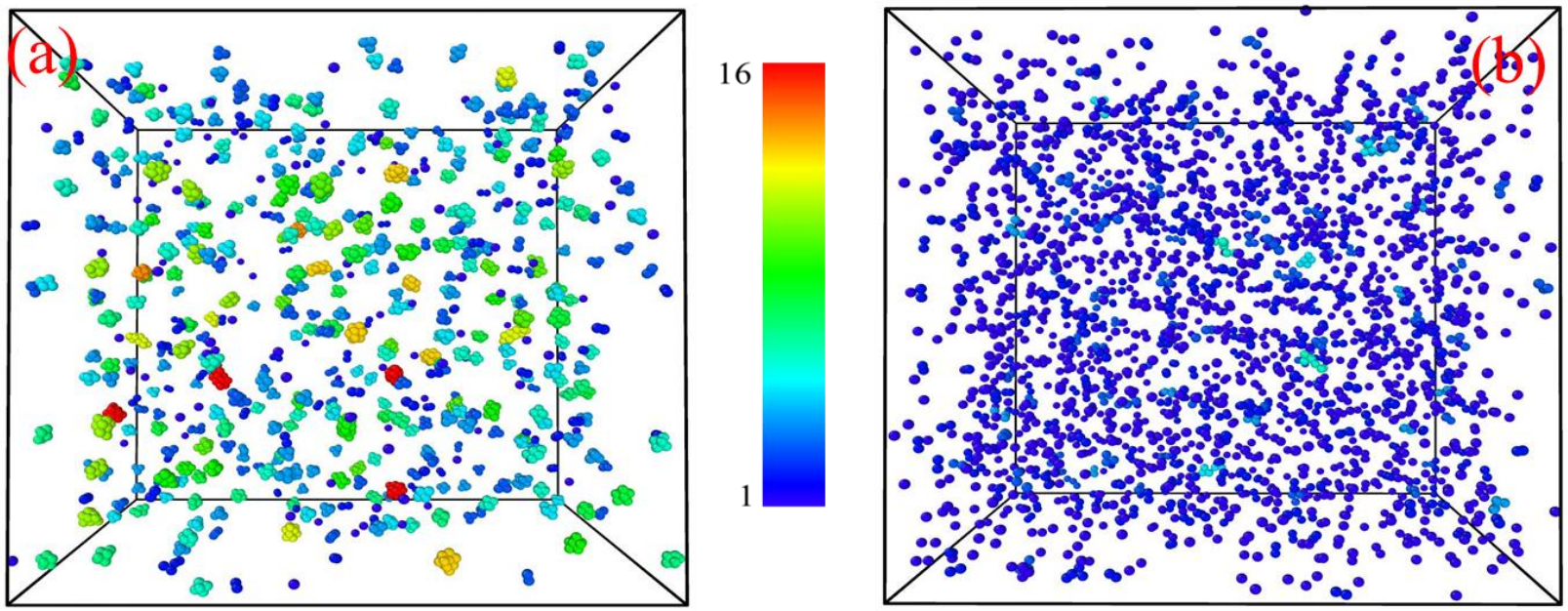

Helium clusters formed in iron (a) and vanadium (b), where the color shows the number of He atoms included in the clusters

Most helium atoms get clustered in iron, but only a few helium atoms clustered in vanadium. Clustering of interstitial helium atoms in Fe is much more obvious than that in vanadium ！

Hu N, Deng H, Hu, W, et al. RSC Advances, 2016, 6(32): 27113-27118.
Hu N, Deng H, Hu, W, et al.. Nuclear Instruments and Methods in Physics Research Section B: Beam Interactions with Materials and Atoms, 2013, 303: 72-74.

Defect production in substitutional-helium doping α-iron under irradiation

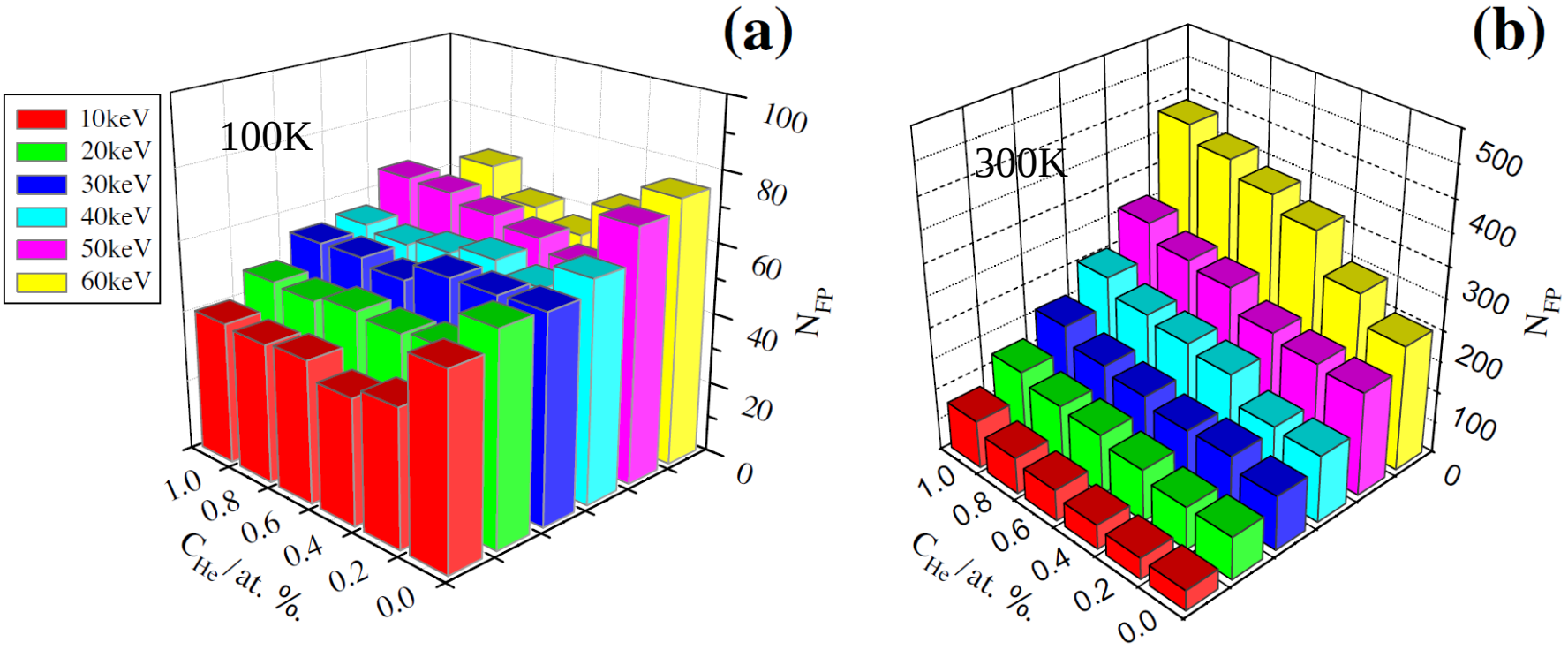

At 100K (a), the production of Frenkel pairs increases with PKA energy increases, but decreases with He content increases;

At 300K (b), the production of Frenkel pairs increases with PKA energy and He content increases

Defect production in substitutional-helium doping α-iron under irradiation

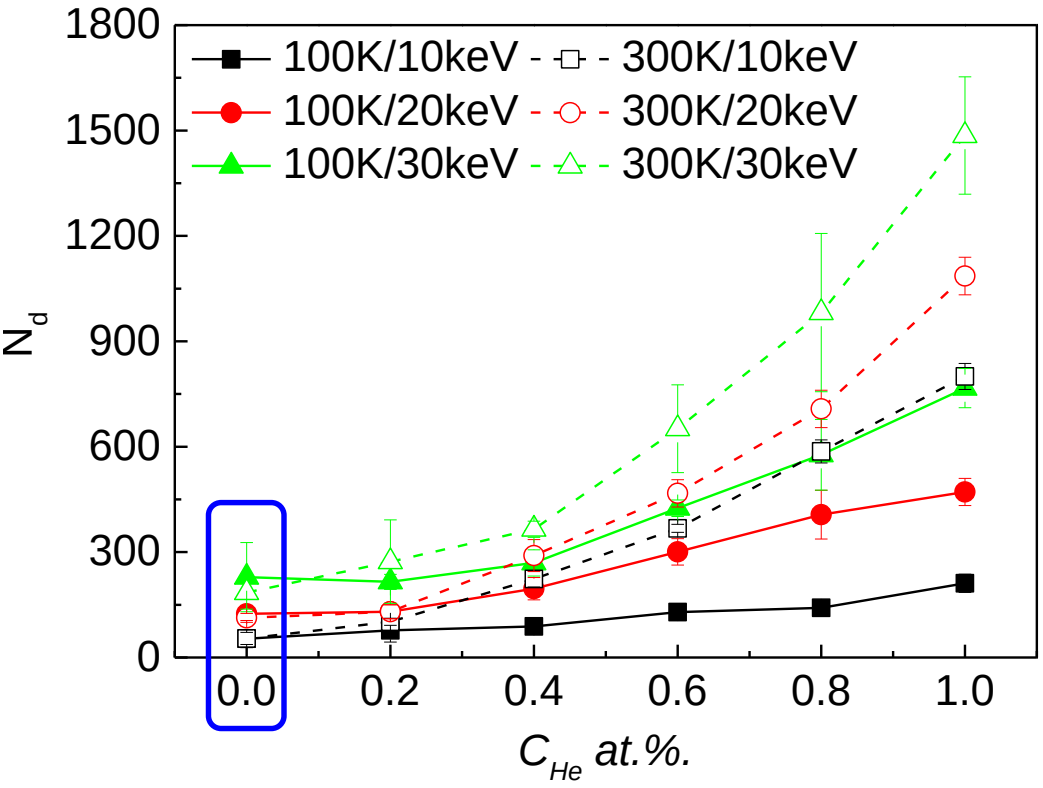

- Number of displacement induced Frenkel pairs increases with he content increases;
- With same He content, the NFP increases with the PKA energy increases;
- With same PKA energy and He content, the number of FPs increases with temperature increases (except for the case C_{He}=0)

The increase of helium atoms increases the number of defects and the increasing rate can be greatly enhanced by the increasing of PKA energy and initial radiation temperature

Defect distribution around displacement cascade region in interstitial-He doping α-Fe

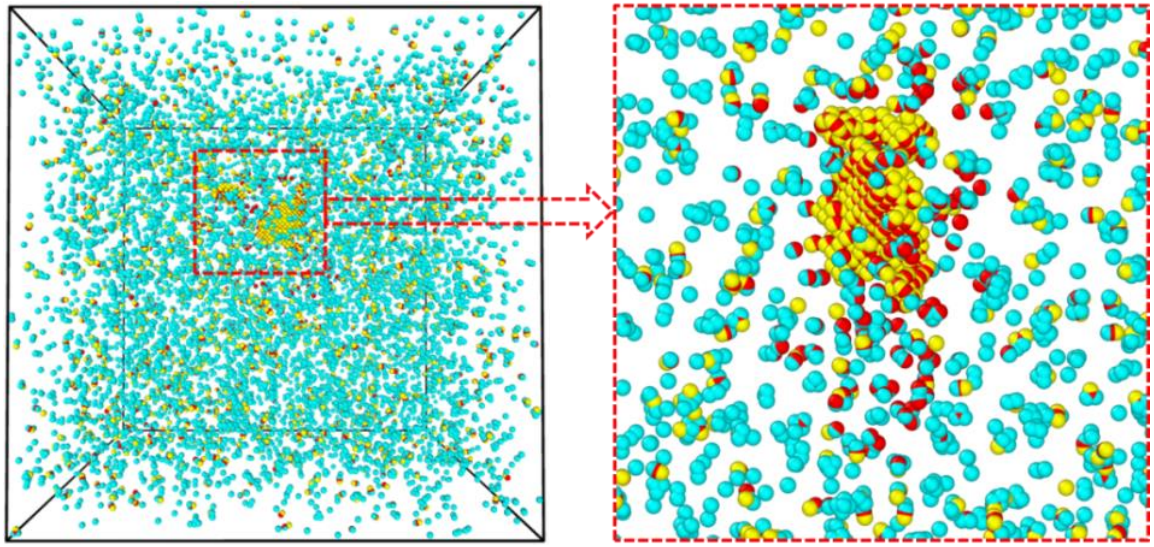

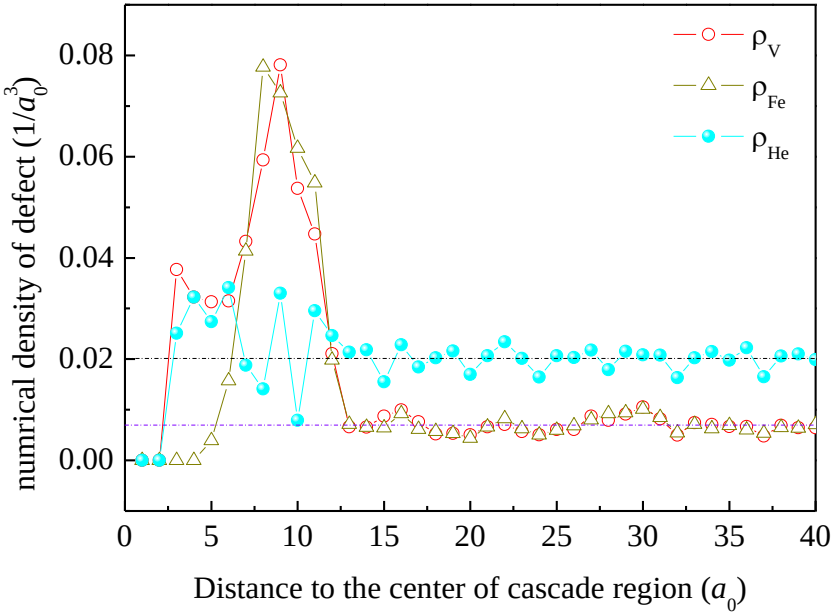

Vacancy SIA and helium defect distribute in different shells around the center of cascade region.

Numerical distribution of all defect clusters in sub-He doping Fe

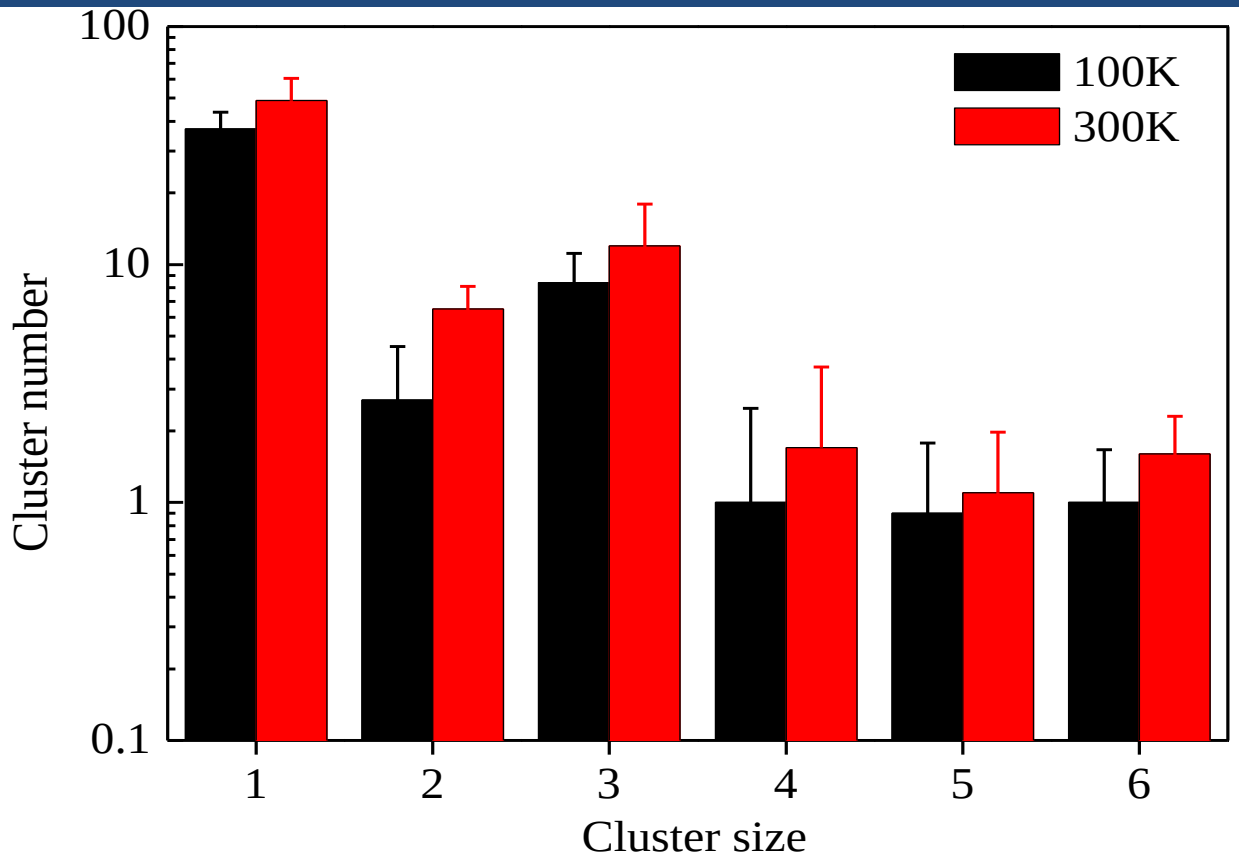

Most defect have clustered into small clusters, the number of clusters decreases with the size of cluster increases, more have clusters formed under higher temperature.

Numerical distribution of all defect clusters in int-He doping Fe

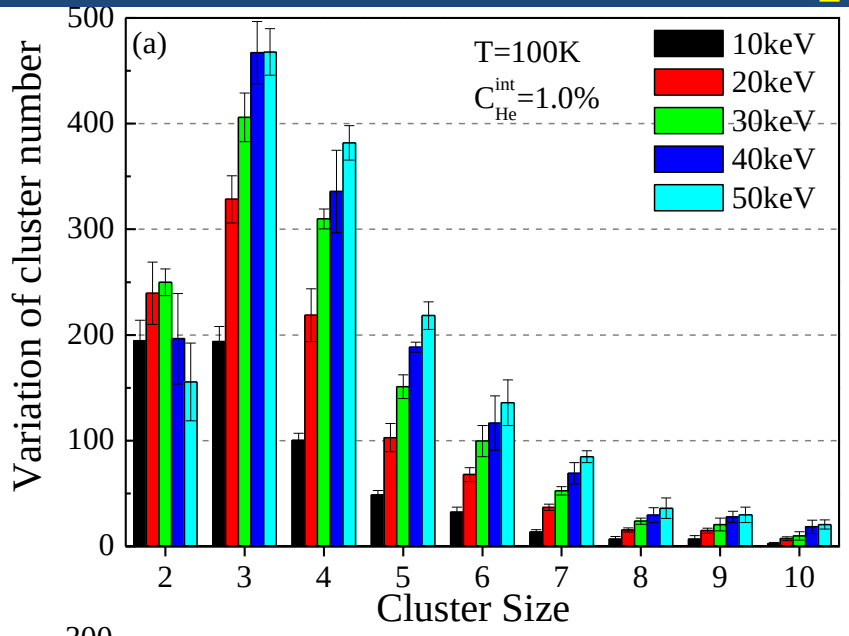

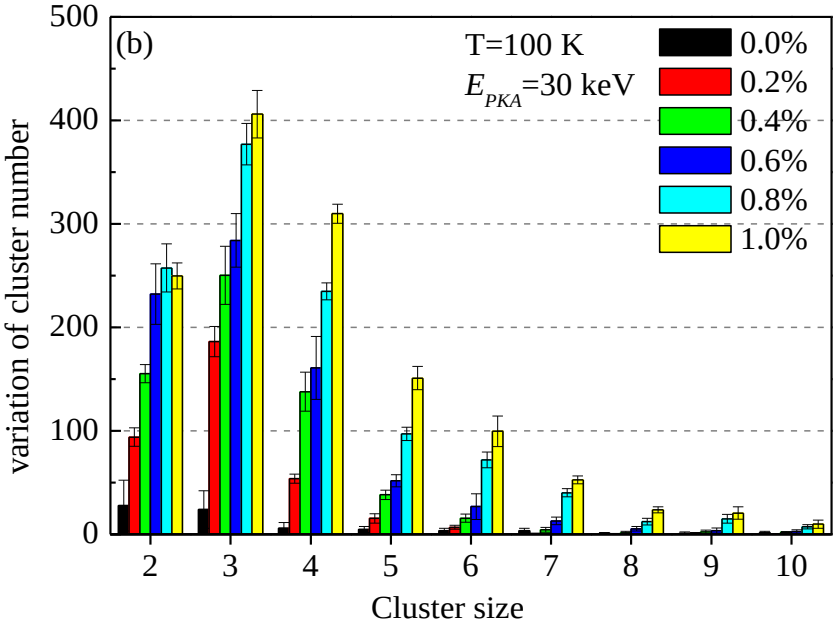

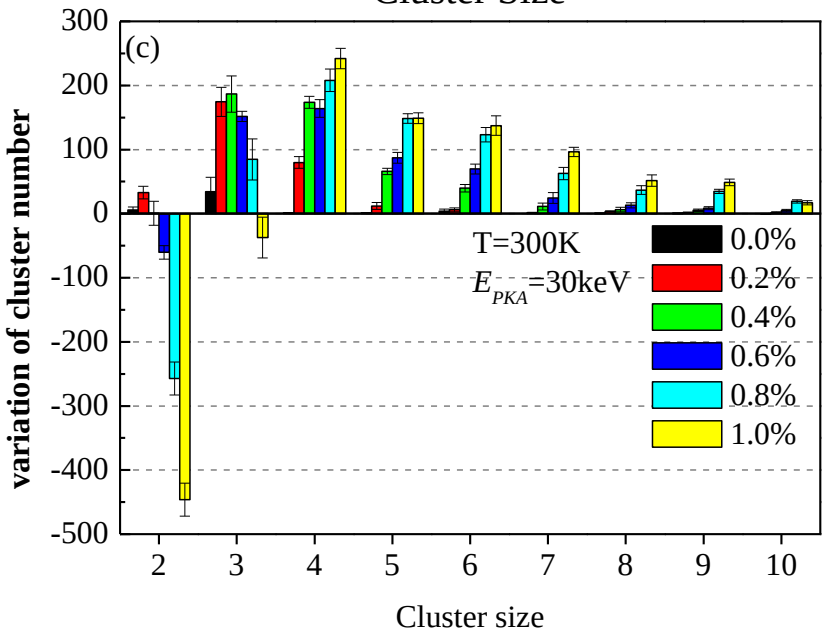

At low size, as the PKA energy and He content increases, the increased number of clusters increases firstly and then decreases.

Net increase of cluster number at larger size increases as the PKA energy and He content increases.

The negative number means disappearing.

The variation of the number of He_n clusters

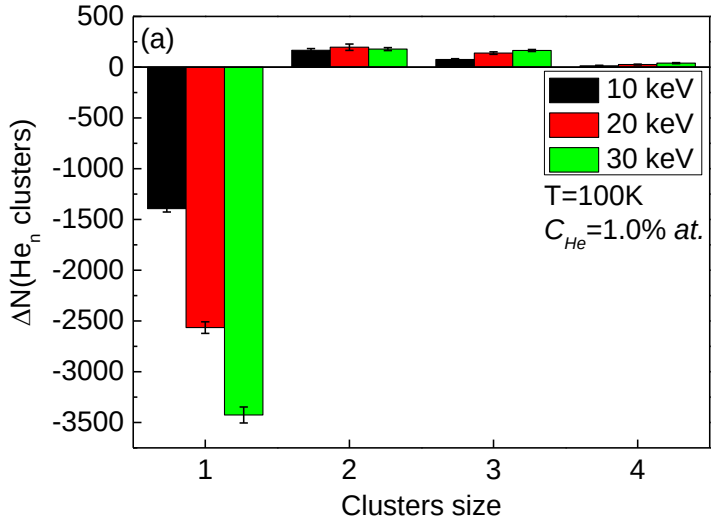

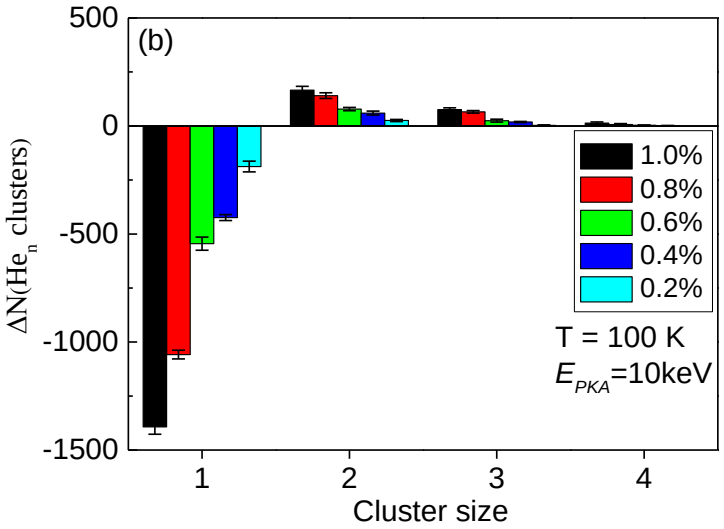

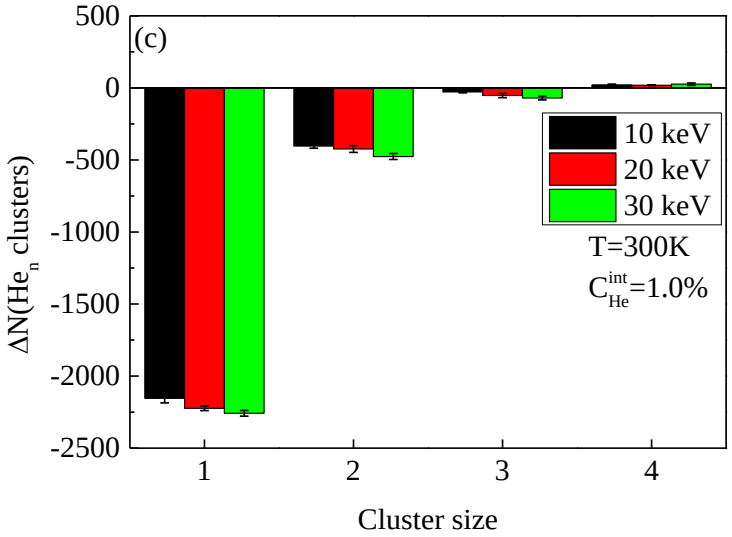

It can be seen that the number of disappeared He_n clusters increases with the increasing of PKA energy and He content at both temperatures;

The increased number of He_n clusters decreases as He content decreases.

The numerical variation of He-Vacancy complexes in iron

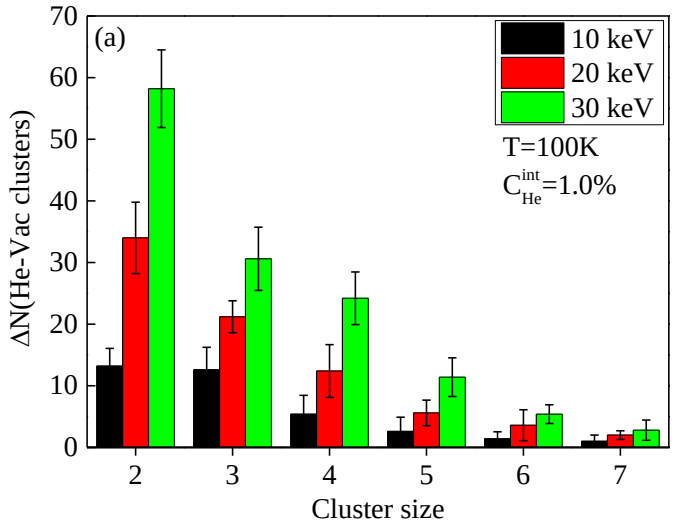

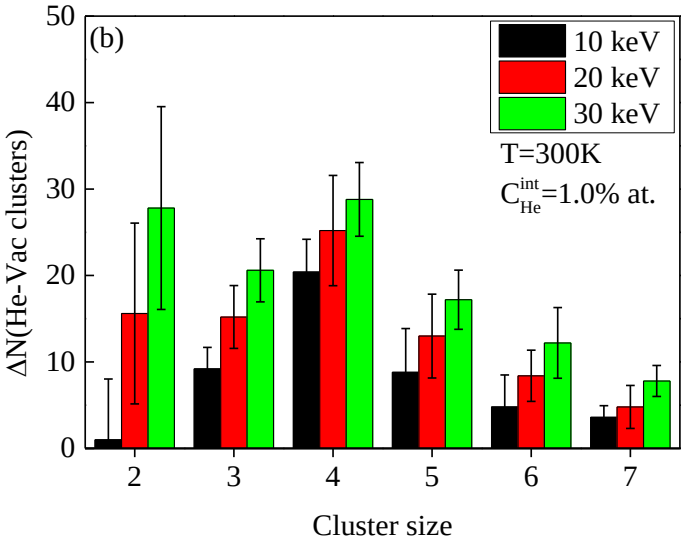

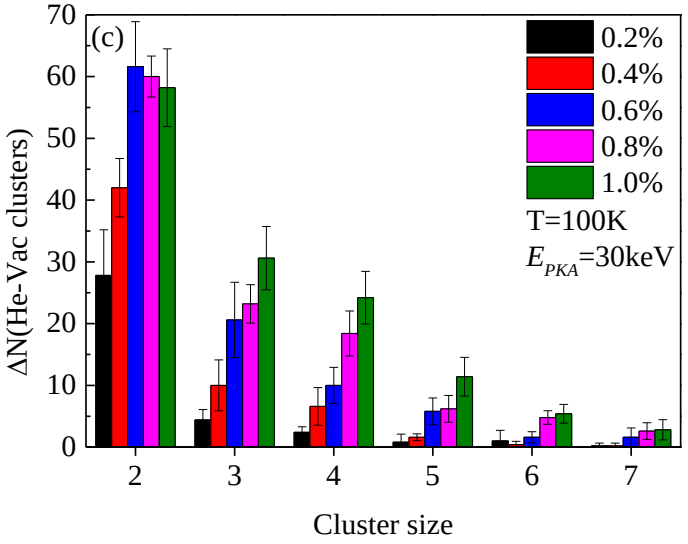

The number of He-Vacancy complexes increases as the PKA energy and He content increases, that is, the increase of PKA energy and He content may effectively promote the clustering between helium atoms and vacancies.

Effect of temperature and He contents on the trapping of He atoms

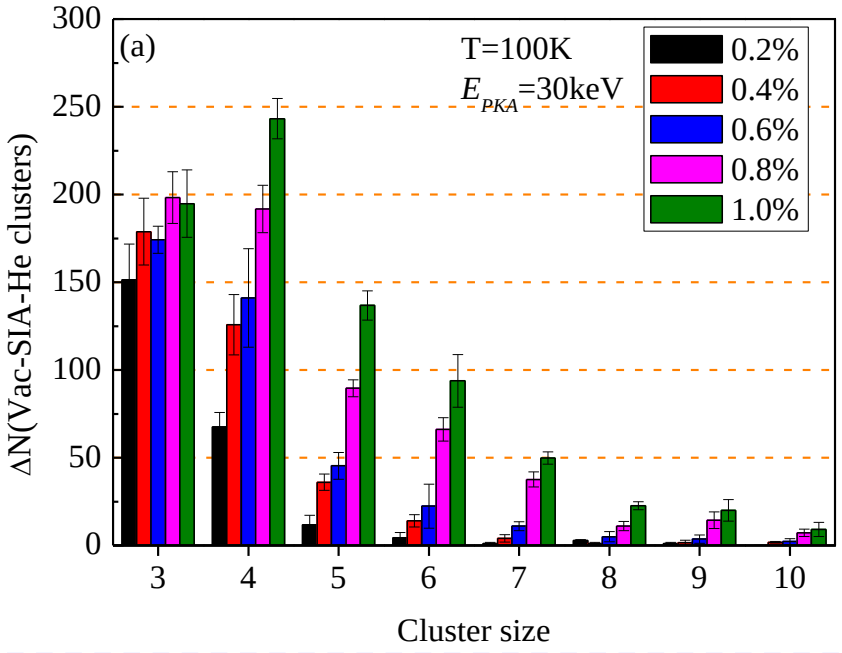

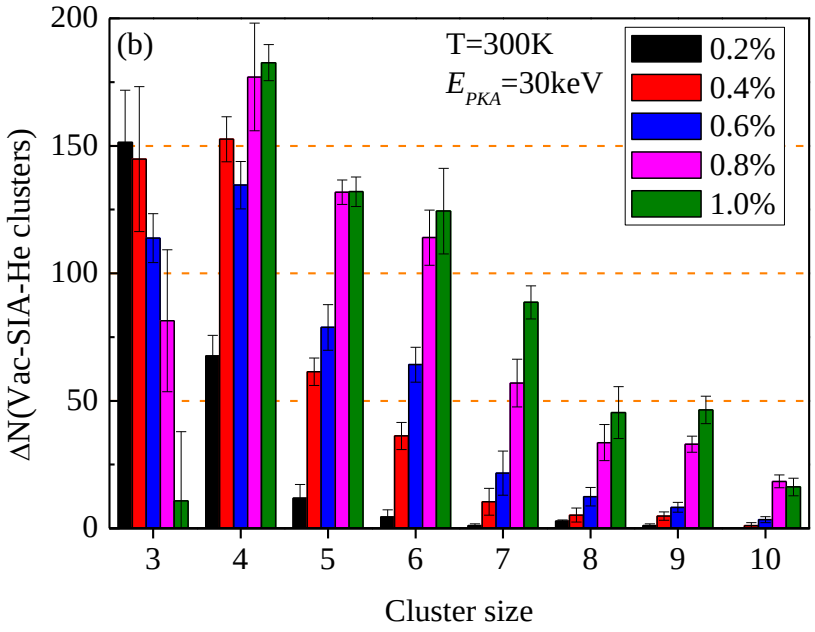

- At 100K, the numerical increasing of small Vac-SIA-He clusters have been promoted by the increase of He content.
- At 300K, the numerical increasing of small Vac-SIA-He clusters have been suppressed by the increase of He content.
- Conclusion: The thermally activated self-trapping is found to be more efficient than collision-induced-defects created capturing.

Backgrounds

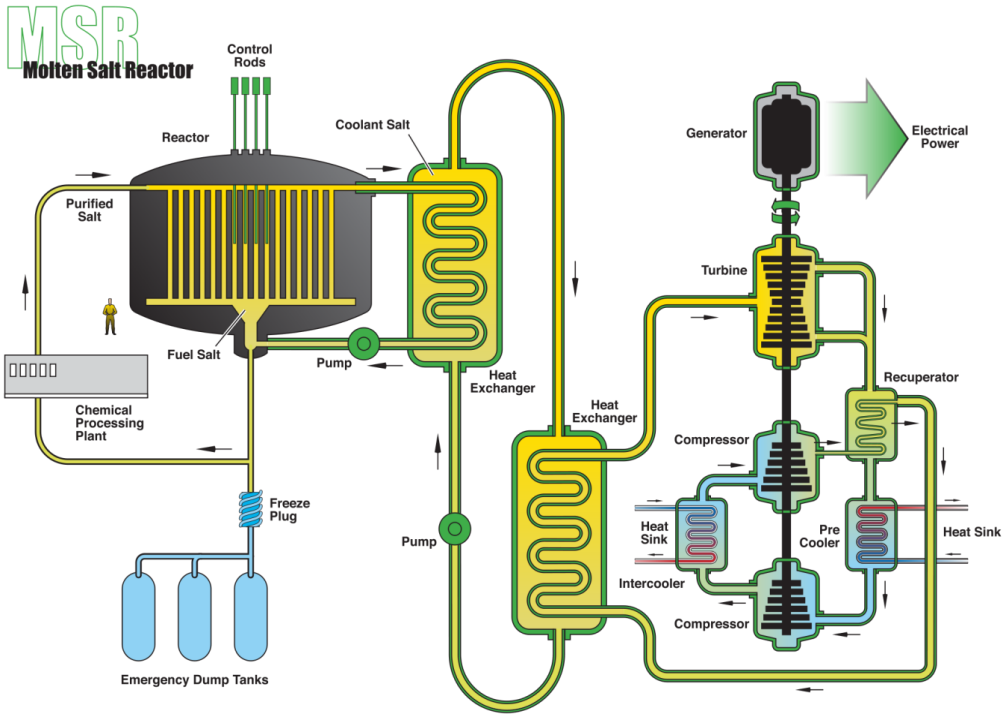

Molten Salt Reactor

- Hastelloy-N has been widely considered as the candidate structural materials in molten-salt reactor for their high performance in resistance to corrosion.
- The predominant composition of Hastelloy-N are Ni, Mo and Cr.

It is meaningful to investigate the irradiation behaviors of hastelloy-N. An binary alloy of Ni-Mo has been simulated with molecular dynamics method.

MD and OKMC simulations of the displacement cascades in nickel

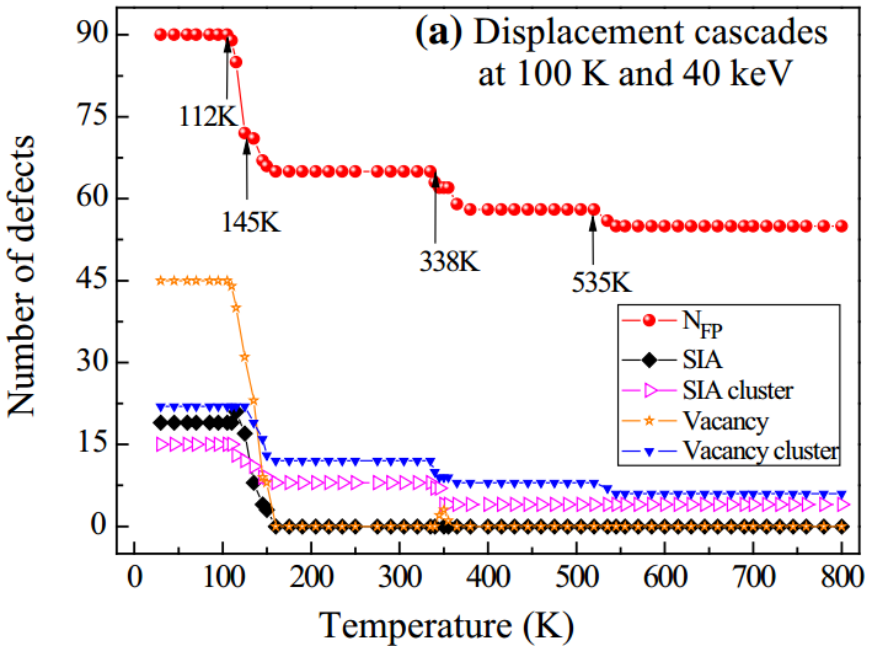

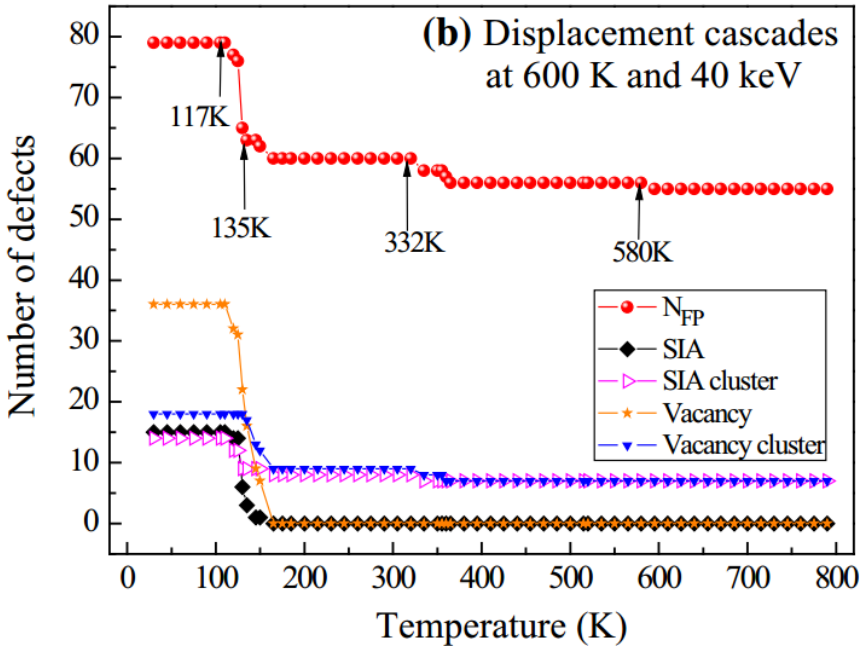

Simulated number of surviving defects in annealing of bulk Ni after displacement cascades at 40 keV at 100 and 600 K

The evolution stages are as follows: Stage I at about 115 K, Stage II at about 350 K, and Stage III at about 550 K.

Xiao W J, Wu G Y, Hu W, et al. MD and OKMC simulations of the displacement cascades in nickel. Nuclear Science and Techniques, 2016, 27(3): 57.

MD and OKMC simulations of the displacement cascades in nickel

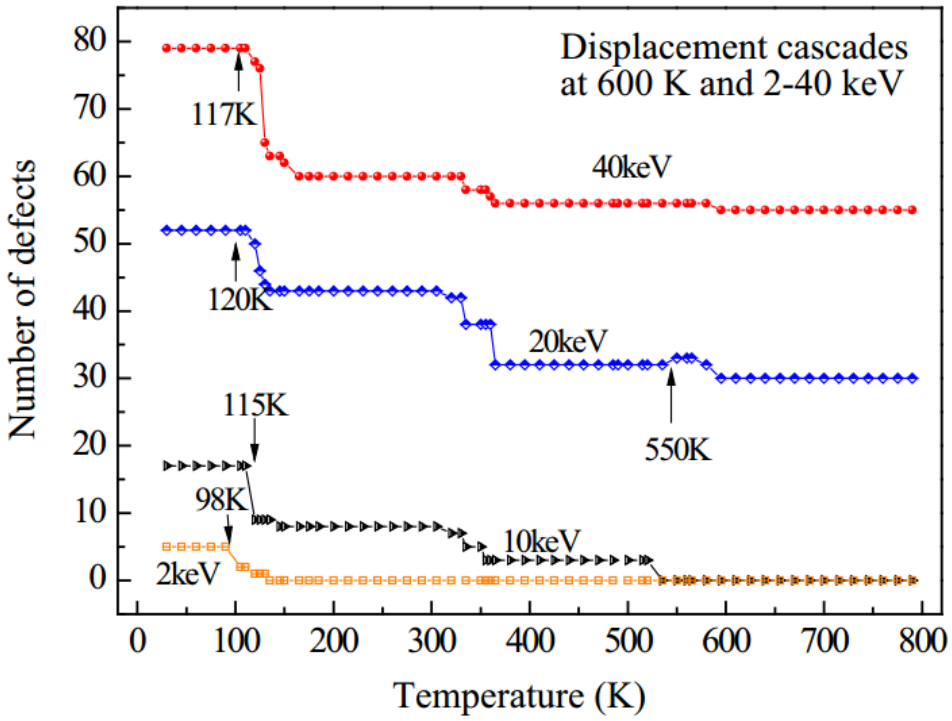

Simulated number of surviving defects in annealing of bulk Ni after displacement cascades at 40 keV at 100 and 600 K

The defects generated in high-temperature cascades are more stable than those in the low-temperature cascades. At $E_{cascade}$<10 keV, almost all the defects annihilate in the annealing process, while at $E_{cascade}$>20 keV, about 60 % of the defects remain after annealing process .

MD and OKMC simulations of the displacement cascades in molybdenum

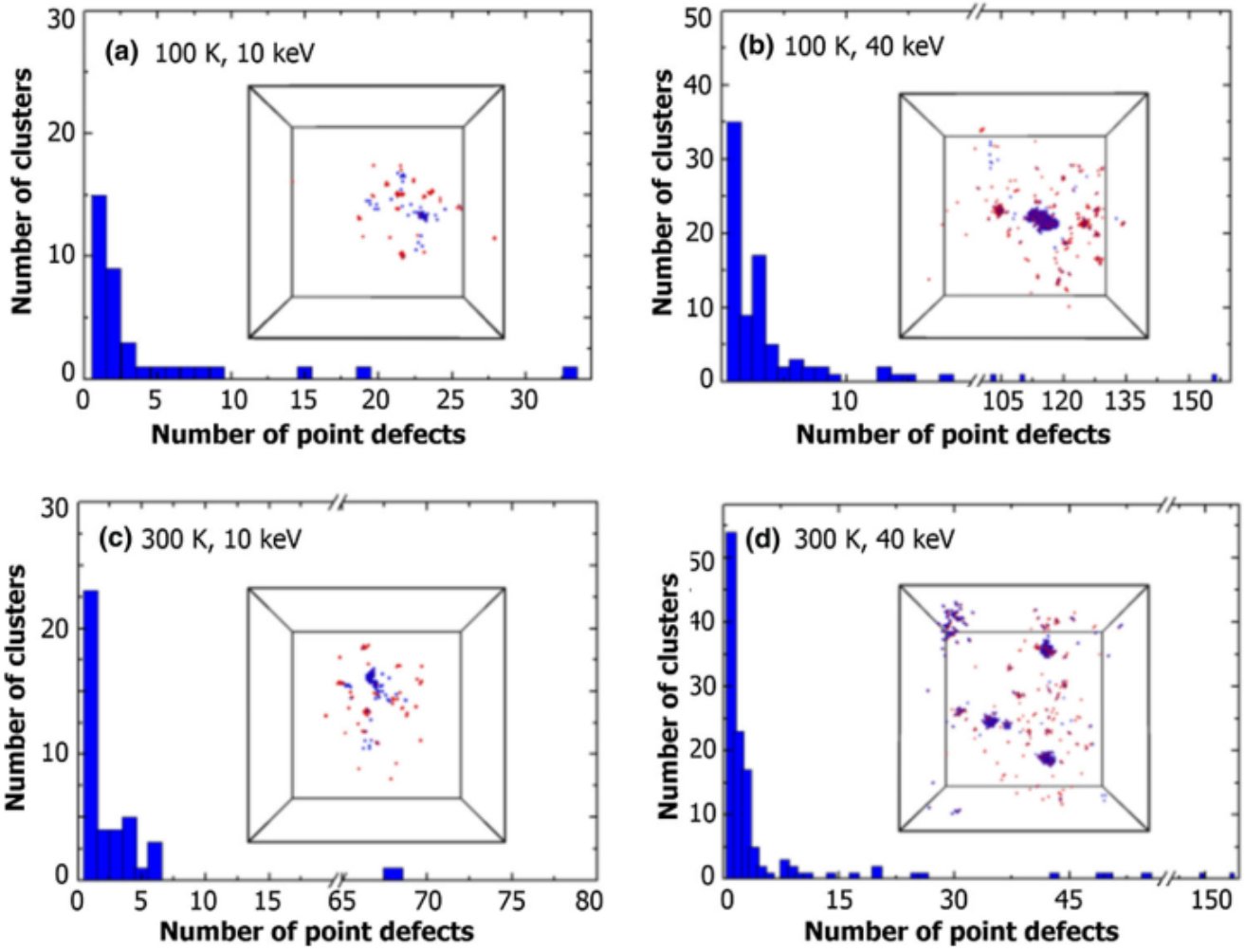

Size distribution of defect clusters at MD temperature of 100 and 300 K and E_{PKA} of 10 and 40 keV. Blue, vacancy; red, interstitial.

Wu G Y, Hu N W, Deng H Q, et al. Simulation of radiation damages in molybdenum by combining molecular dynamics and OKMC. Nuclear Science and Techniques, 2017, 28(1): 3.

MD and OKMC simulations of the displacement cascades in molybdenum

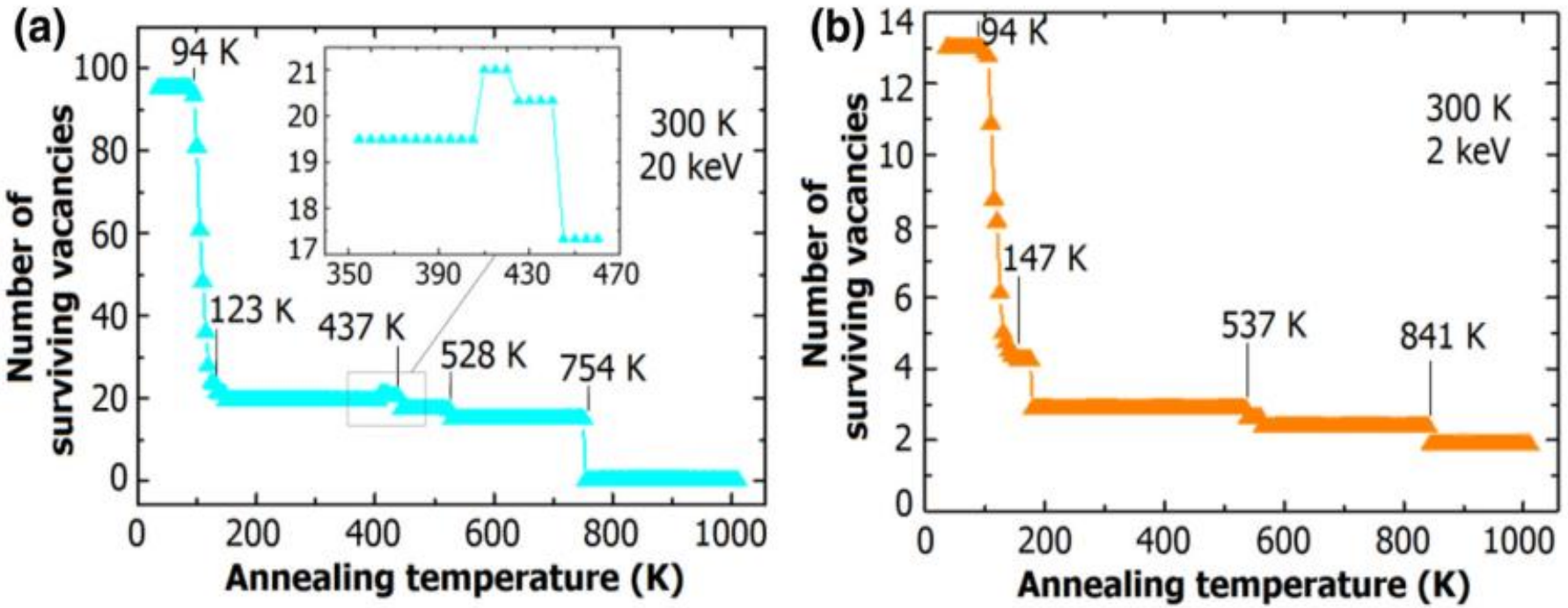

Residual number of vacancies versus the annealing temperature, for primary defects at 300 K and E_{PKA} = 2 and 20 keV

The small clusters generated at E_{PKA} = 2 keV completely recombine in Stage I, but larger clusters recombine at high temperatures

MD and OKMC simulations of the displacement cascades in molybdenum

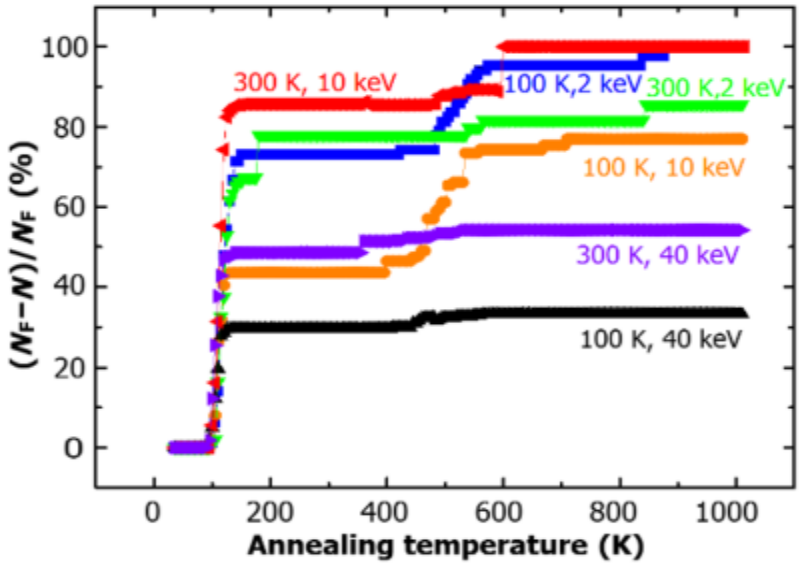

Fraction of recovery defects as function of annealing temperature for E_{PKA} = 2, 10 and 40 keV

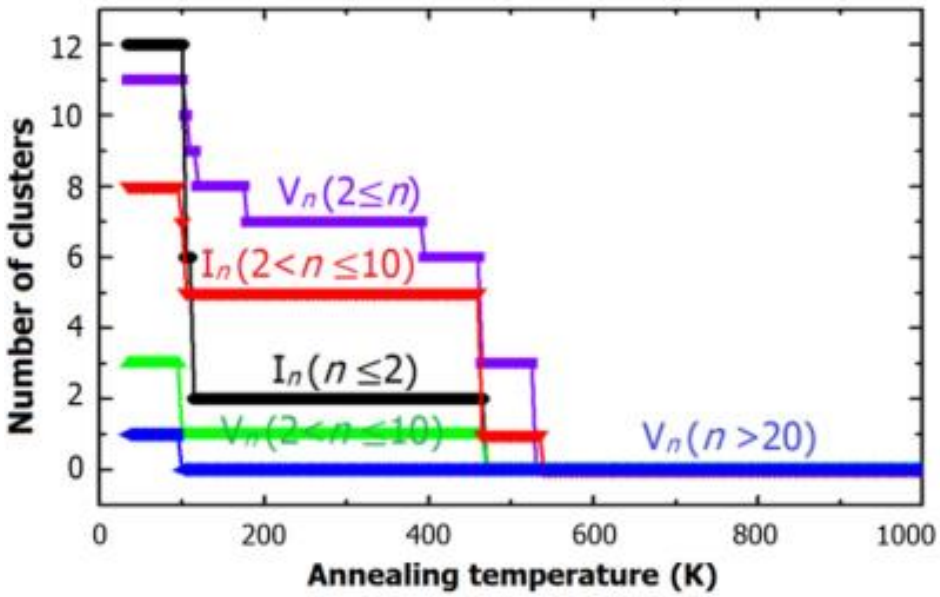

Average number of species clusters versus annealing temperature for PKA energy of 10 keV

MD simulation of displacement cascade in Ni-Mo binary alloys

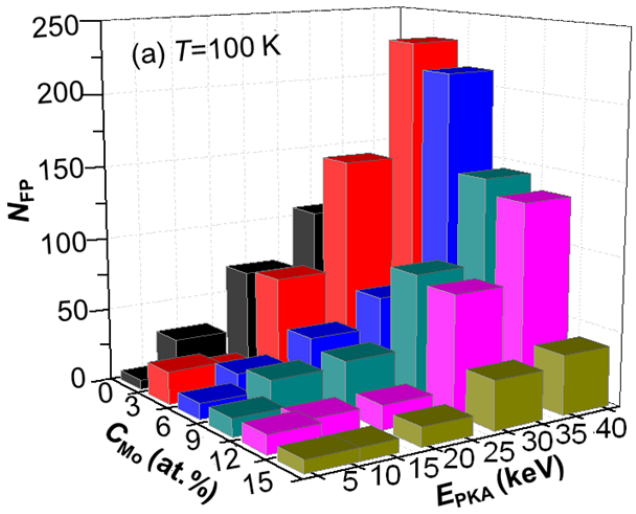

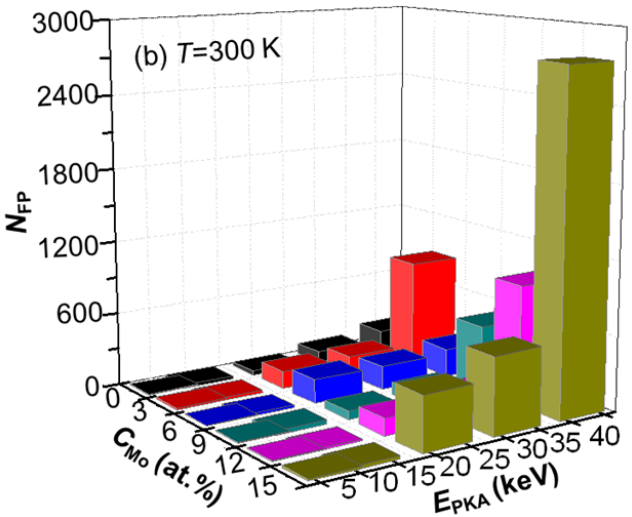

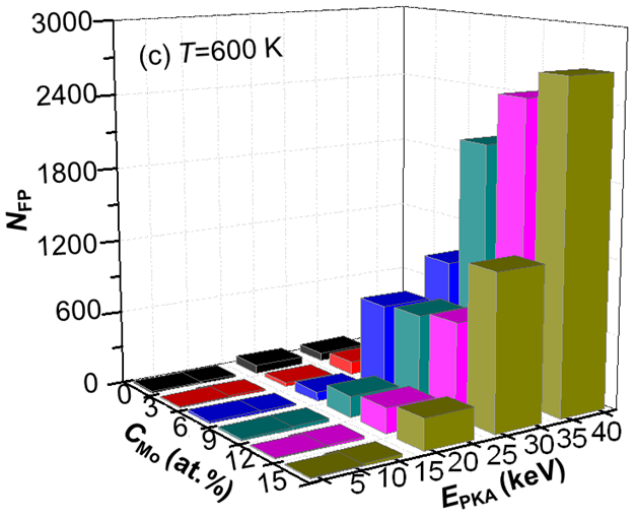

The number of defects generated in displacement cascades caused by PKAs of 5-40 keV in NiMo alloy at (a)100 K, (b)300K and (c) 600 K.

The number of defects resulting from cascade collisions decreases slightly with increasing atomic concentrations of Mo at 100 K. However, it increases rapidly with C_{Mo} at 300K and 600 K. Mo atoms play an opposite role in defect generation, they prevent defect generations at low temperatures but enhance them at higher temperatures.

MD simulation of displacement cascade in Ni-Mo binary alloys

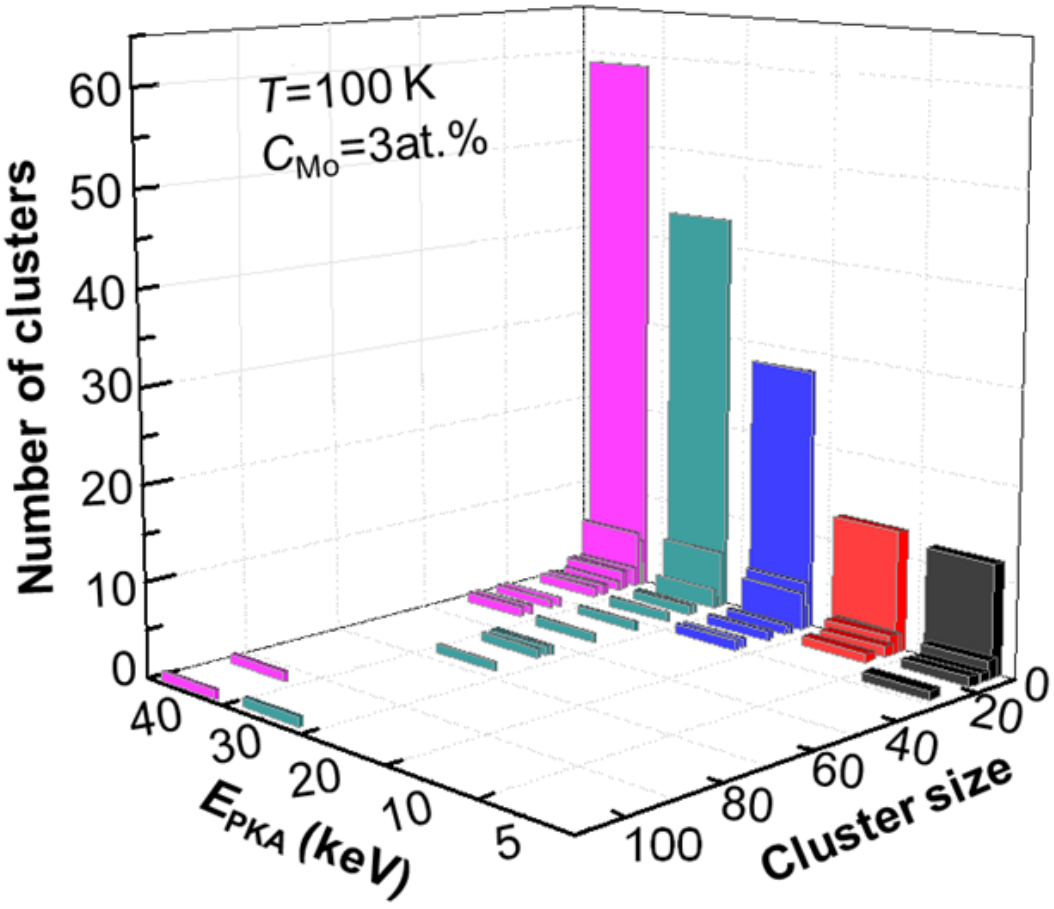

The number of defects cluster as function of the defect cluster size and the PKA energy

Most defects generated in cascade processes distribute in clusters and the number of small cluster increases with PKA energy.

The increasing number of small clusters is due to that high energy PKAs may generate high temperature zones, where interstitials and vacancies are easier to migrate and aggregate.

MD simulation of displacement cascade in Ni-Mo binary alloys

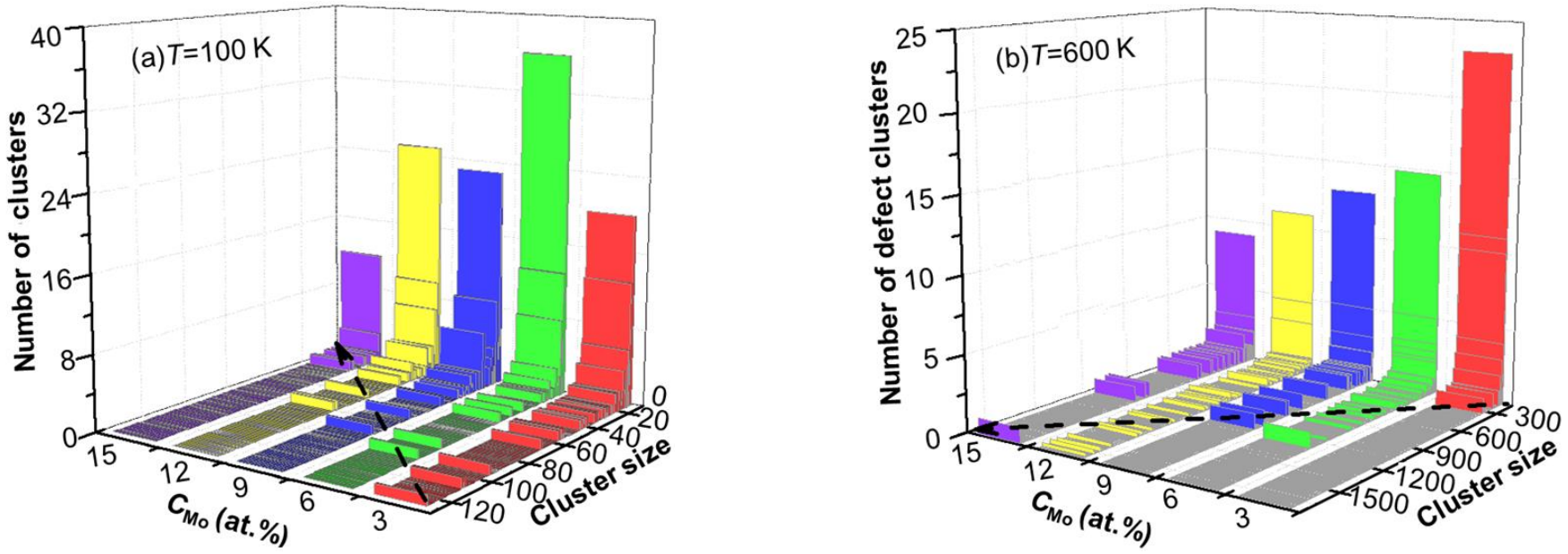

Distribution of defect cluster number as the functions of cluster size and the concentration of solute Mo atoms at 100K (a) and 600 K(b). The number of defect clusters generated at C_{Mo} =3.0at.% and 100K includes all clusters formed for each PKA energy.

The number of small clusters decreases slightly with increasing C_{Mo}. The size of the largest clusters in Ni-Mo alloy decreases with increasing atomic concentrations of Mo at 100 K, while it increases sharply with the Mo content at 600 K.

The evolution of displacement defects studied with Kinetic Monte Carlo (KMC)

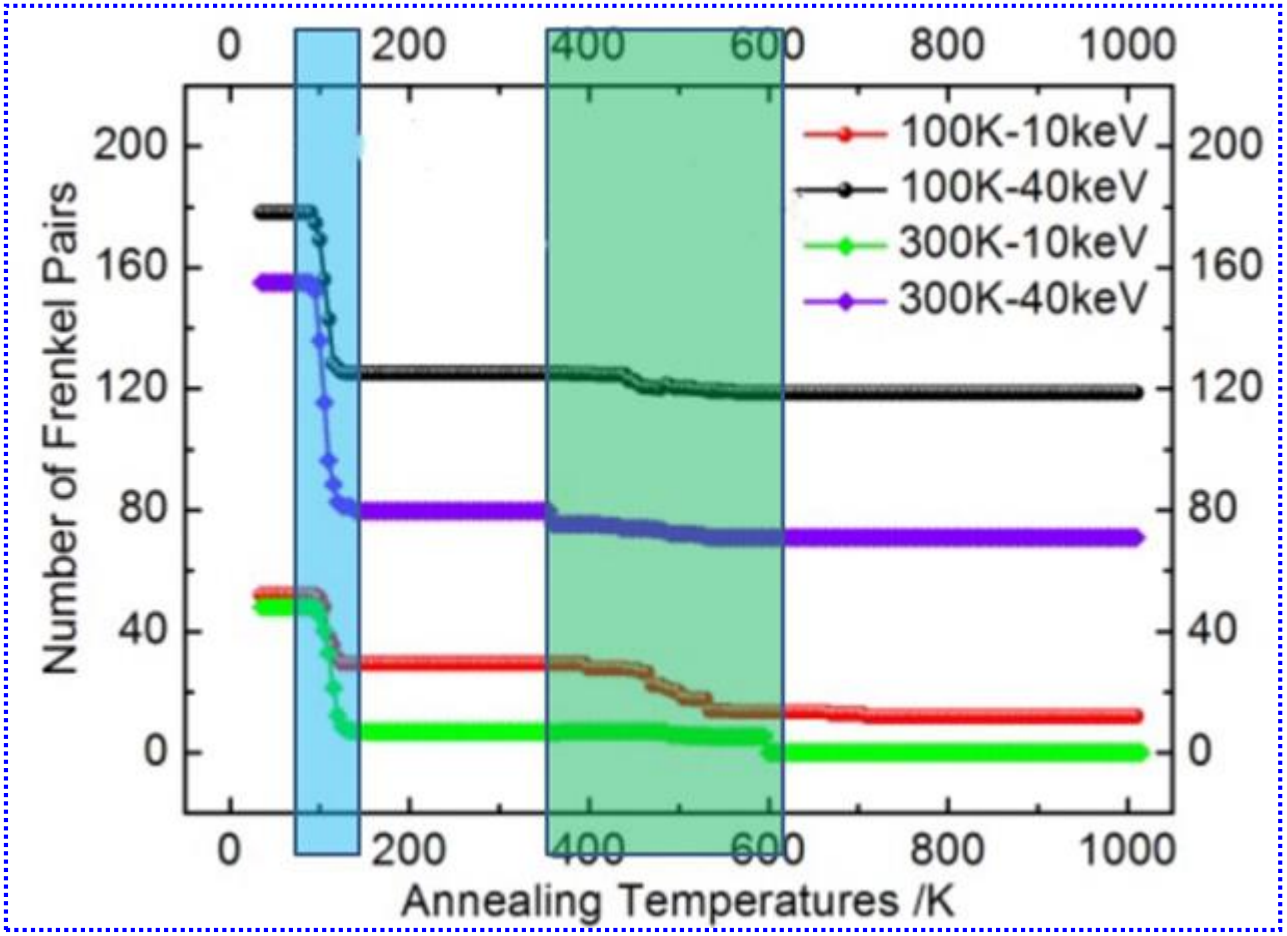

Defect production in substitutional-helium doping bcc vanadium under irradiation

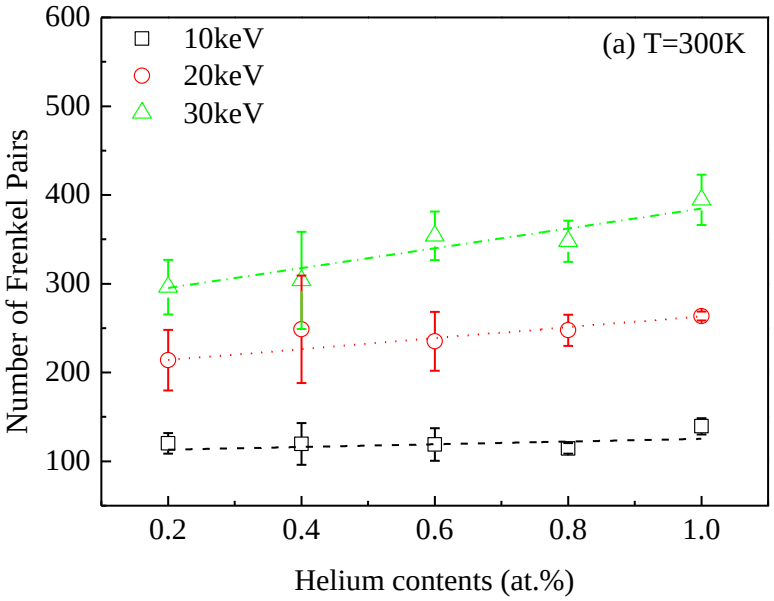

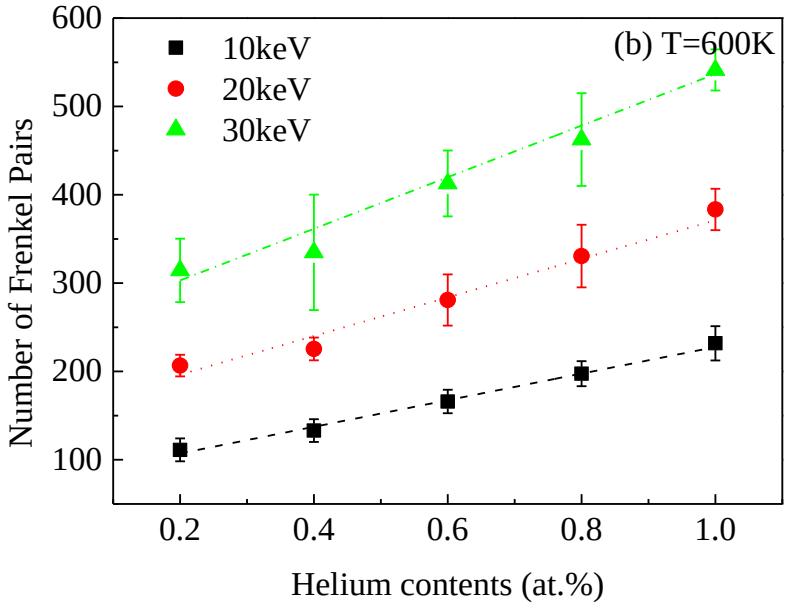

At both temperatures ((a) 300K and (b) 600K), the increase of either helium concentration or PKA energy increase the production of defects, higher temperature leads to larger generation rate.

Defect production in substitutional-helium doping bcc vanadium under irradiation

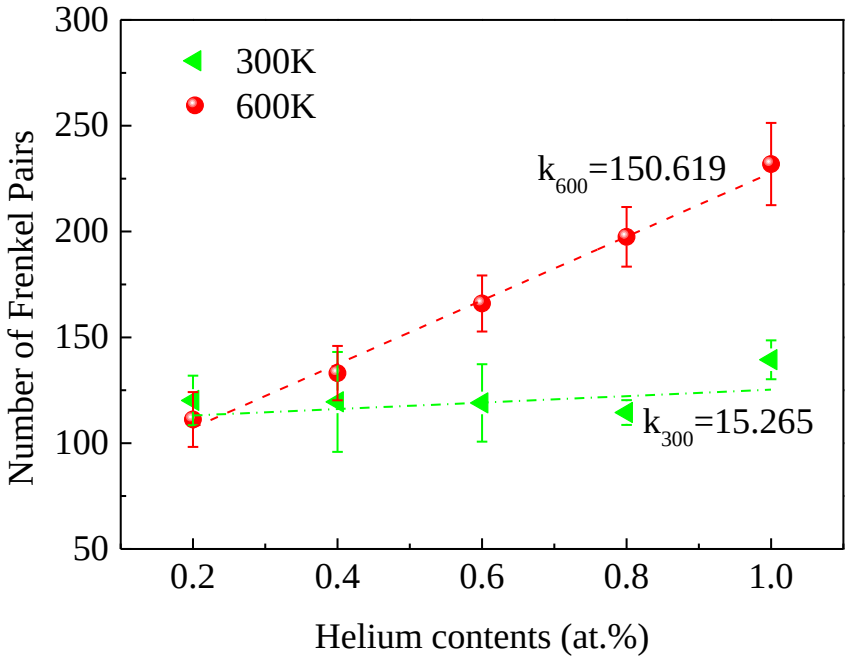

- The number of Frenkel pairs can be fitted as a linear function of Helium contents at both 300 and 600 K.
- The increasing rate of FPs, the fitted slope increases with temperature increases.

PKA energy	Environment temperature	
	300 K	600 K
10 keV	k = 15.265	k =150.619
20 keV	k = 61.640	k =218.426
30 keV	k =111.784	k =292.058

Defect production in substitutional-helium doping bcc vanadium under irradiation

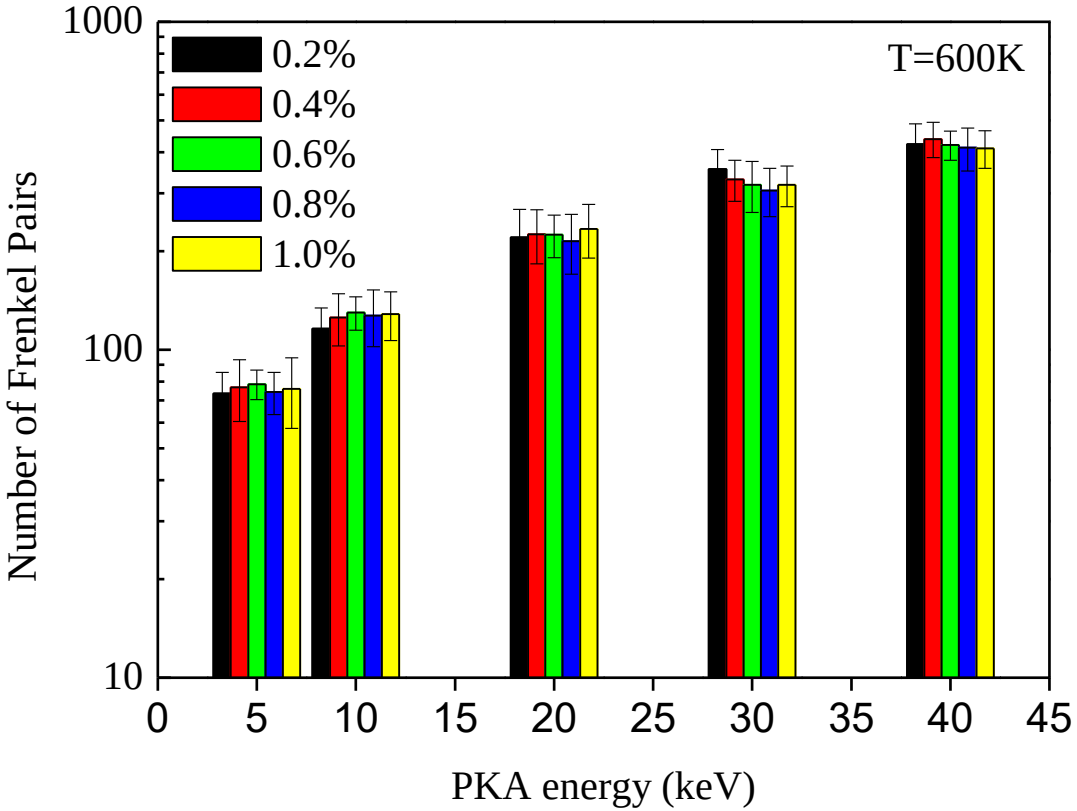

The number of Frenkel pairs increases with the increase of He content when He content is not larger than 0.6%, however, when the He content is larger than 0.6%, the production of Frenkel pairs decreases with the increase of He content.

Defect distribution around displacement cascade region in interstitial-He doping vanadium

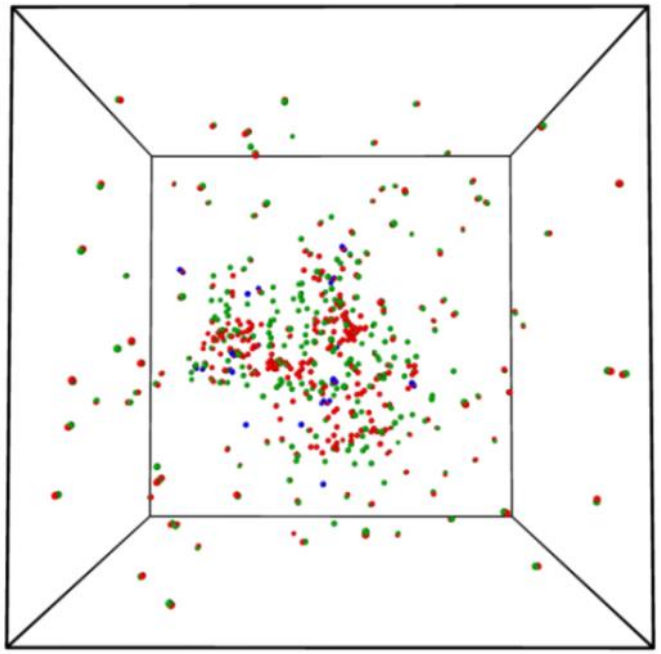

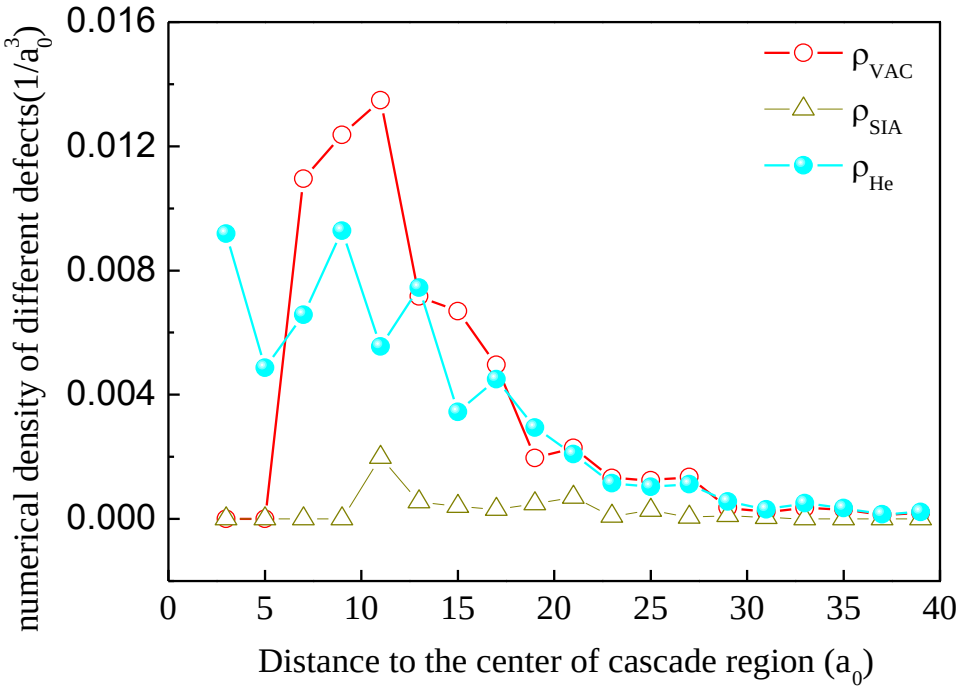

Only a few SIAs form in the cascade region but do not distribute in the exact center of this region, vacancies and helium defects distribute in the center

Numerical variation of cascade defects in sub-He doping vanadium

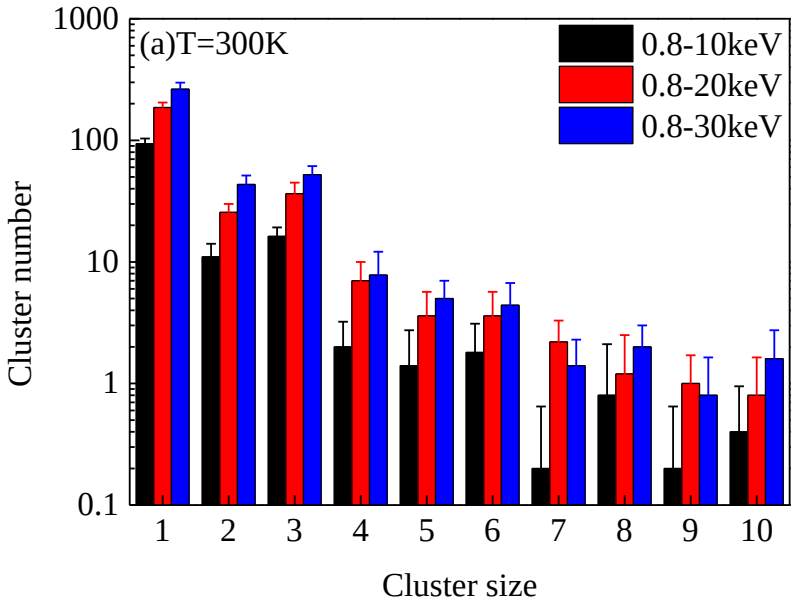

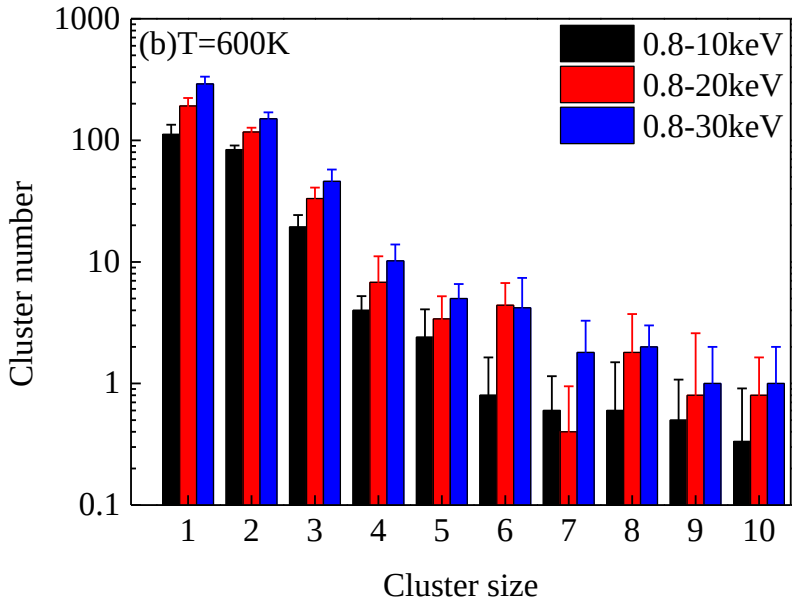

At both 300 and 600K, the increased number of clusters increase with the increasing of PKA energy, but decreases as the size of cluster increases.

Numerical variation of He-vacancy clusters in V-He binary system

C_{He}=1.0%

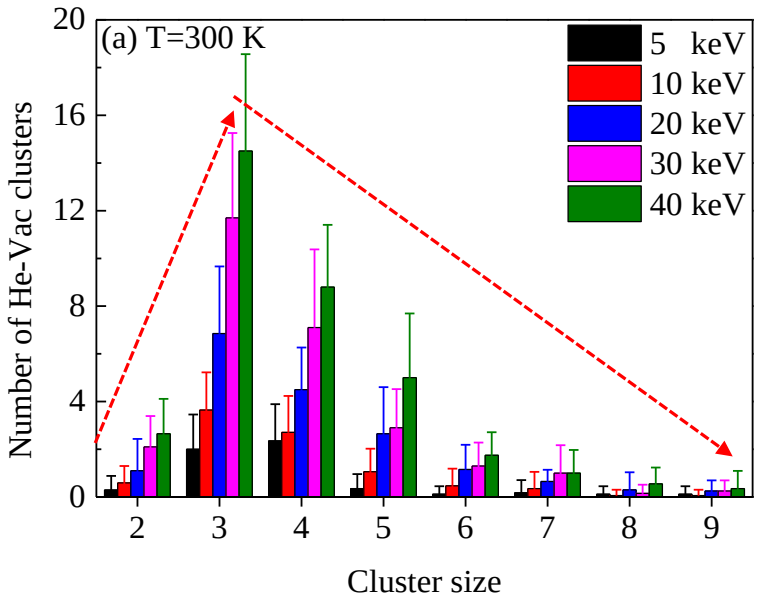

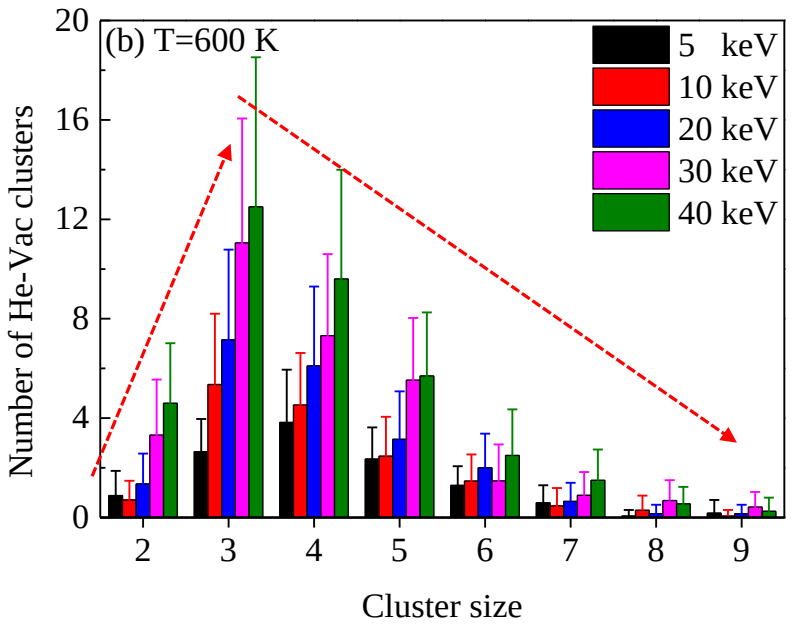

The generation of He-vacancy clusters can be obviously promoted by the increase of PKA energy; it increases firstly and then decreases as the cluster size increases.

Numerical variation of He-vacancy clusters in V-He binary system

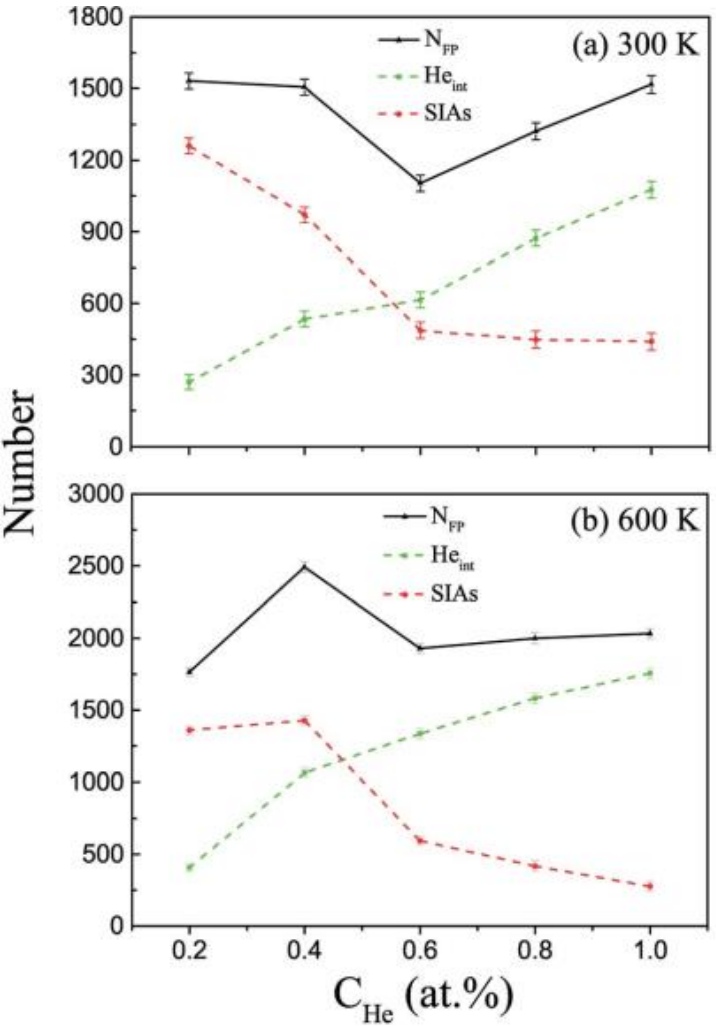

Number of He-int, SIAs, and N_{FP} as a function of C_{He} with PKA energy of 30 keV at (a) 300 K and (b) 600 K.

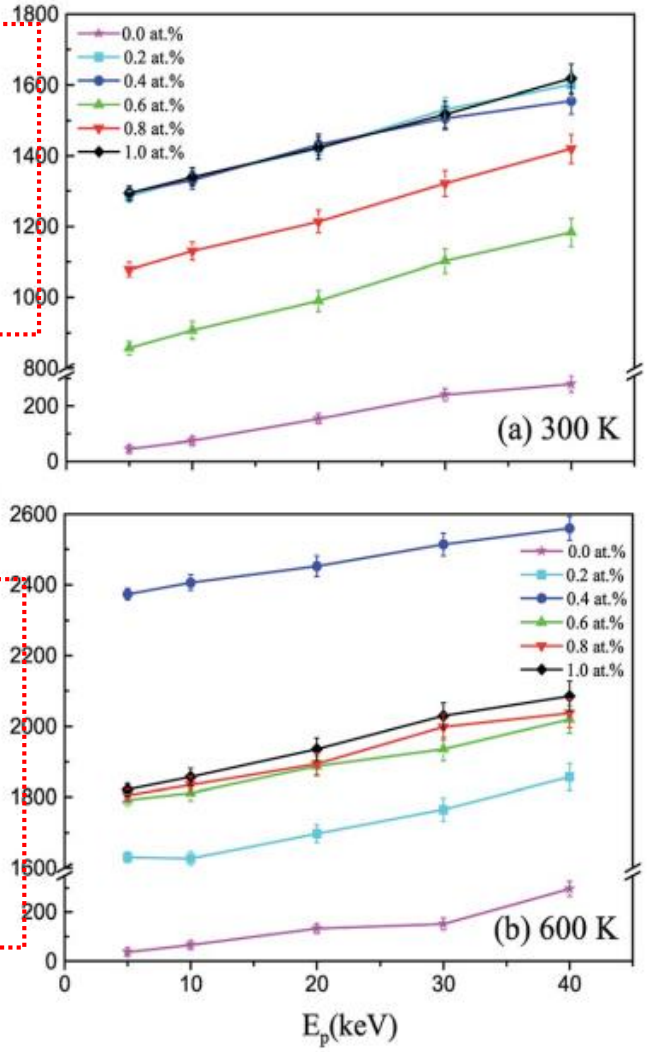

Number of Frenkel pairs N_{FP} as a function of Ep for different He concentrations at (a) 300 K and (b) 600 K

Zhu X, Wang C, Hu W, et al. RSC Advances, 2016, 6(84): 80939-80945.

Numerical variation of He-vacancy clusters in V-He binary system

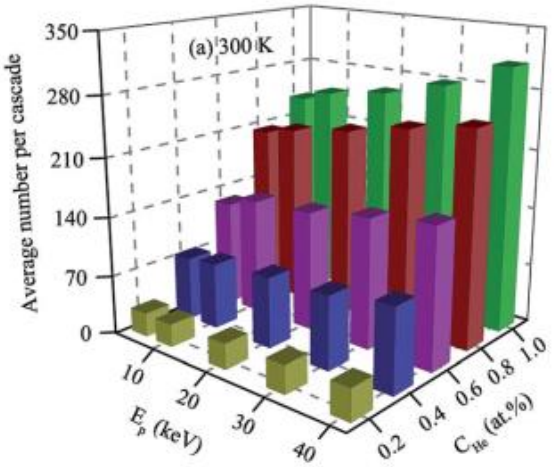

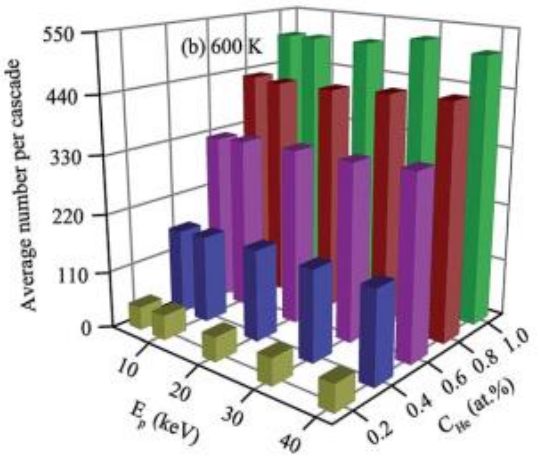

Average number of He-vacancy clusters per cascade vs. *E*p and C_{He} at (a) 300 K and (b) 600 K.

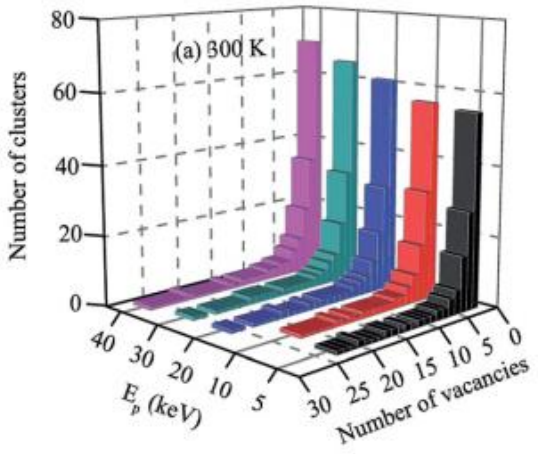

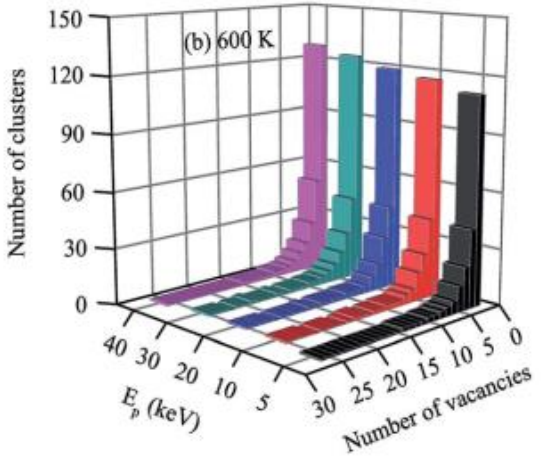

Size distribution of vacancies in He-vacancy clusters with a He concentration of 1.0 at% at (a) 300 K; (b) 600 K.

Numerical variation of He-vacancy clusters in V-He binary system

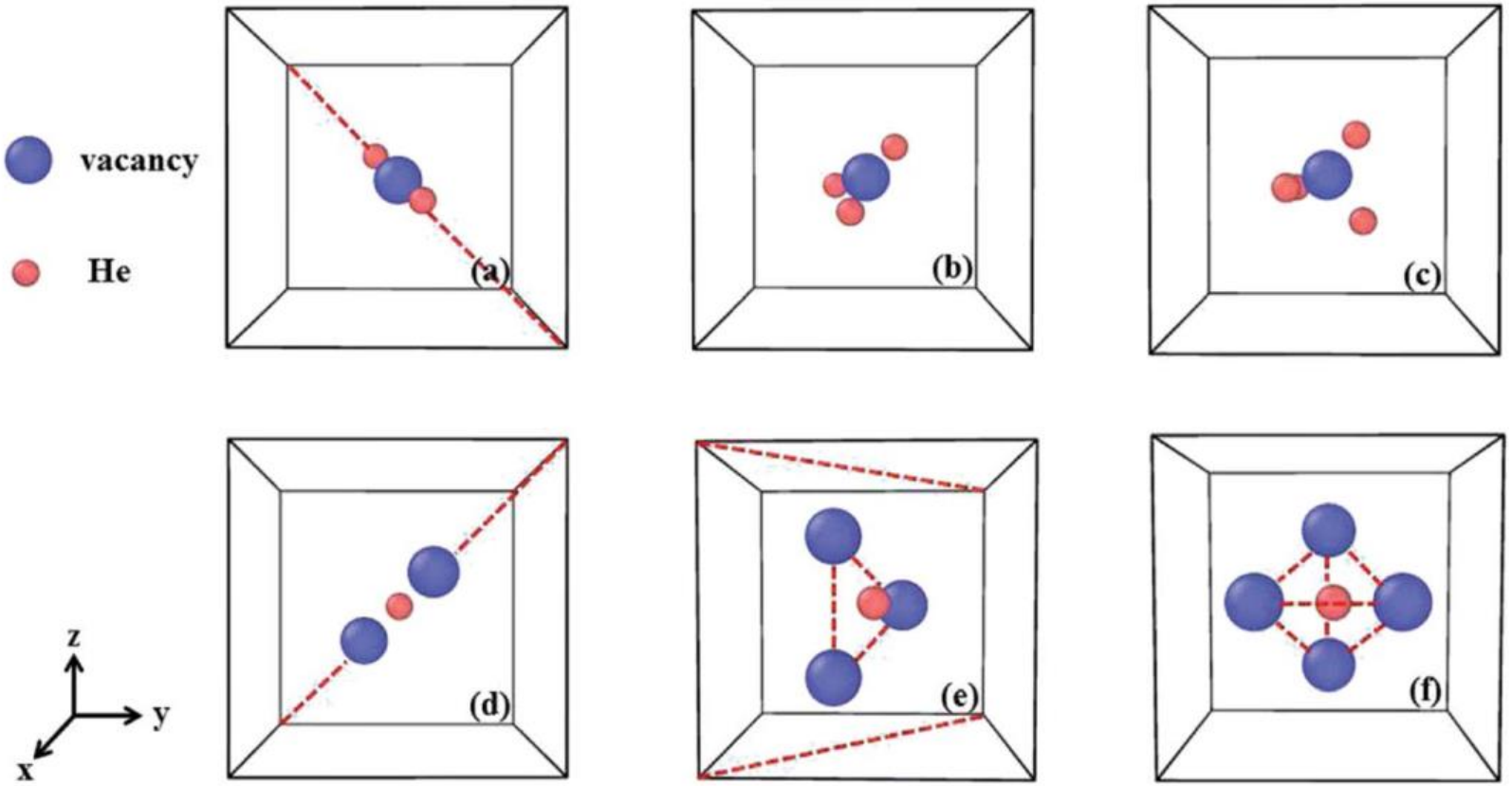

Configurations of six small He-vacancy clusters, as shown in (a) He2V, (b) He3V, (c) He_4V, (d) HeV_2, (e) HeV_3, and (f) HeV_4

Numerical variation of He-vacancy clusters in V-He binary system

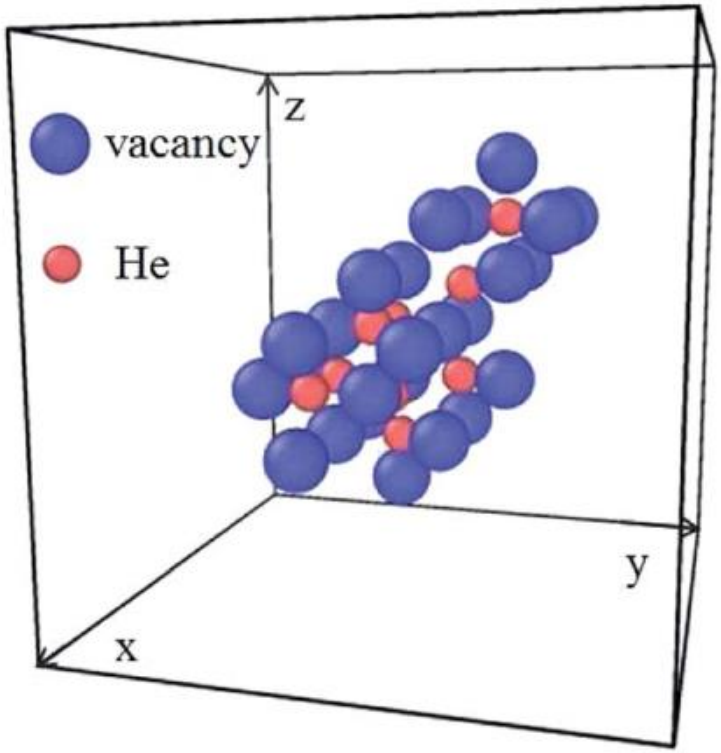

A typical configuration of He_9V_{26} obtained from a 40 keV cascade with a He concentration of 1.0 at% at 600 K.

the interstitial He atoms are located near the tetrahedral sites, rather than the octahedral sites. This indicates that the interstitial He atoms prefer to stay at tetrahedral sites due to the lower formation energy .

MD simulation of displacement cascade in tungsten

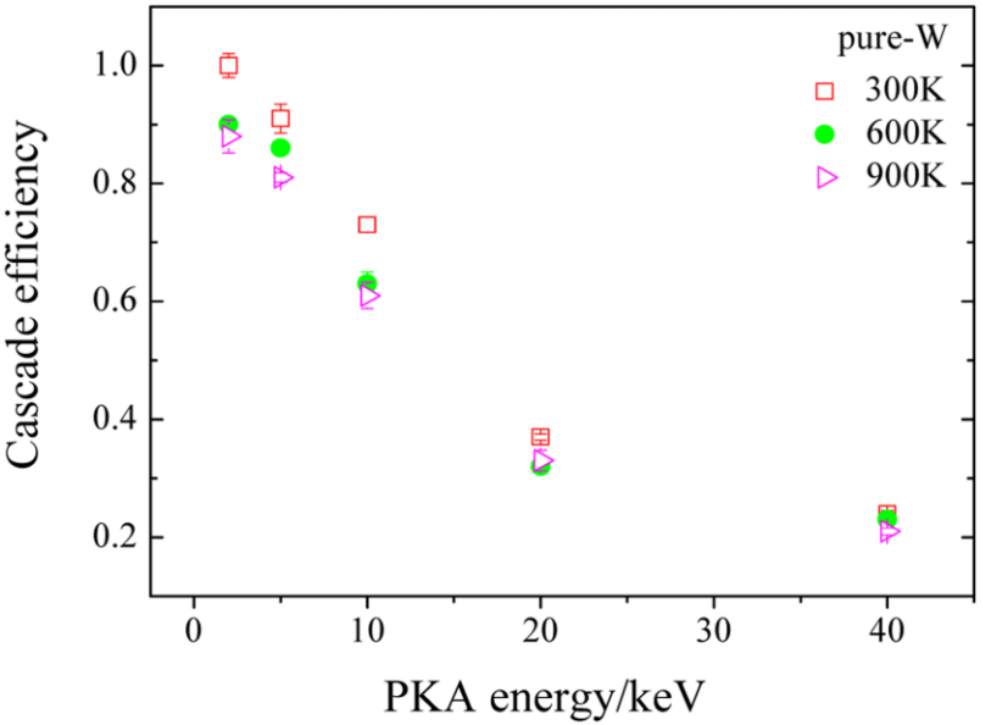

the cascade efficiency in pure W is less than 1.0 under the conditions of all the simulated PKA energies, which means that the total number of Frenkel pairs in bulk W obtained from our simulations is lower than that predicted by the NRT formula at high PKA energy.

The cascade efficiency varies with the PKA energy increasing in pure W at 300 K, 600 K and 900 K, respectively

Yang X, Deng H, Hu W, et al. Molecular dynamics simulation of the displacement cascades in tungsten with interstitial helium atoms. Fusion Science and Technology, 2014, 66(1): 112-117.

MD simulation of displacement cascade in tungsten

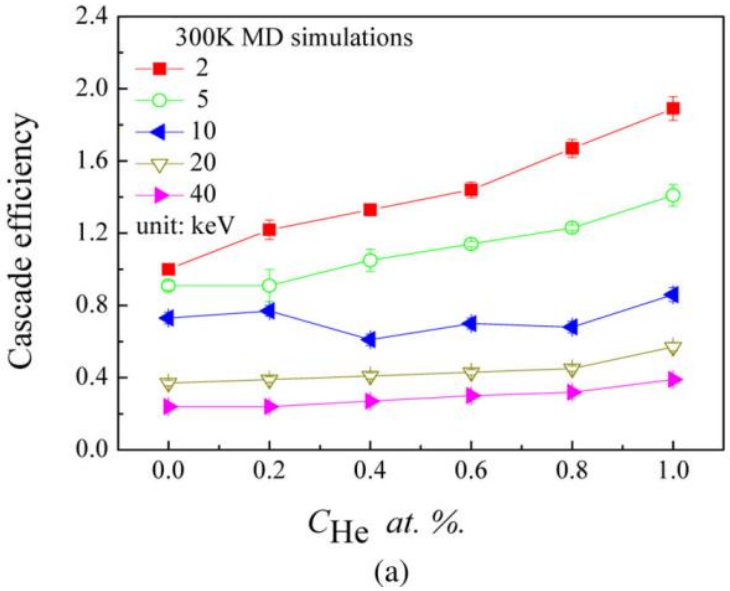

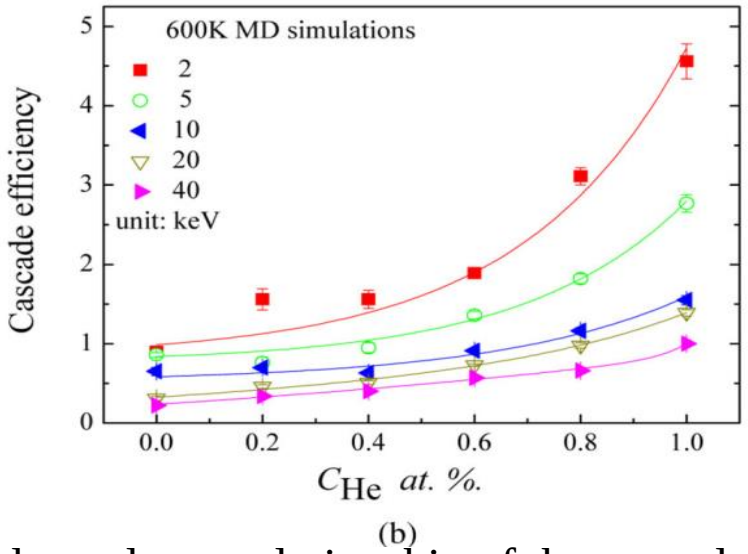

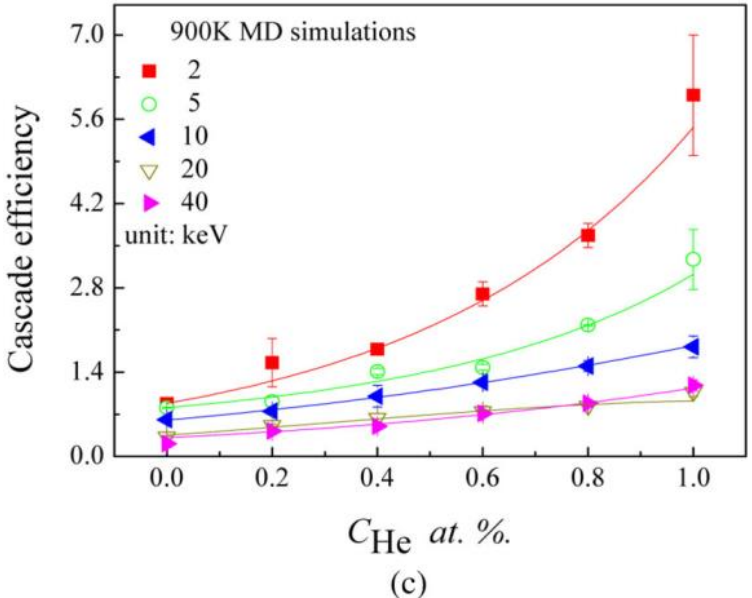

The dependence relationship of the cascade efficiency with respect to NRT model on He concentration (C_{He}) at 300 K(a), 600 K(b) and 900 K(c) under the condition of different PKA energies .

Based on the NRT model and MD simulations, the cascade efficiency has been obtained and it increases with the increasing of interstitial He concentrations.

MD simulation of displacement cascade in tungsten

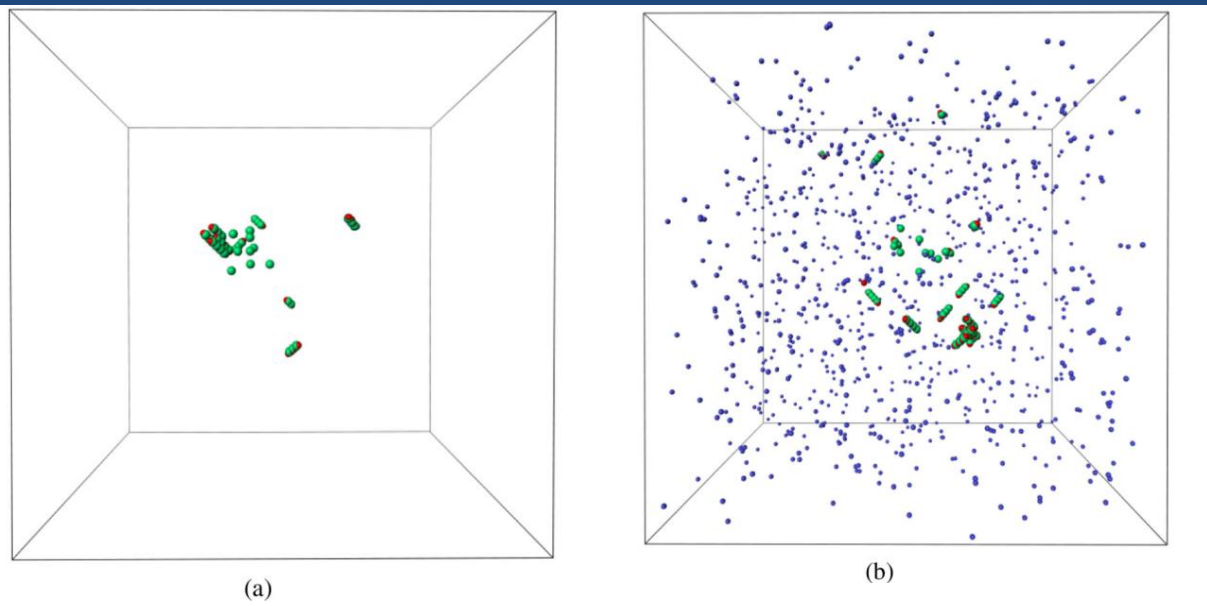

The pictures above show the final structures of defects caused by PKAs with the energy of 40 keV at 900 K. The interstitial He concentration correspond to (a) 0.0 at.%, (b) 0.2 at.%, (c) 0.6 at.% and (d) 1.0 at.%. The red (medium), blue (small) and green (large) balls represent the SIAs, He atoms and vacancies, respectively.

MD simulation of displacement cascade in amorphous

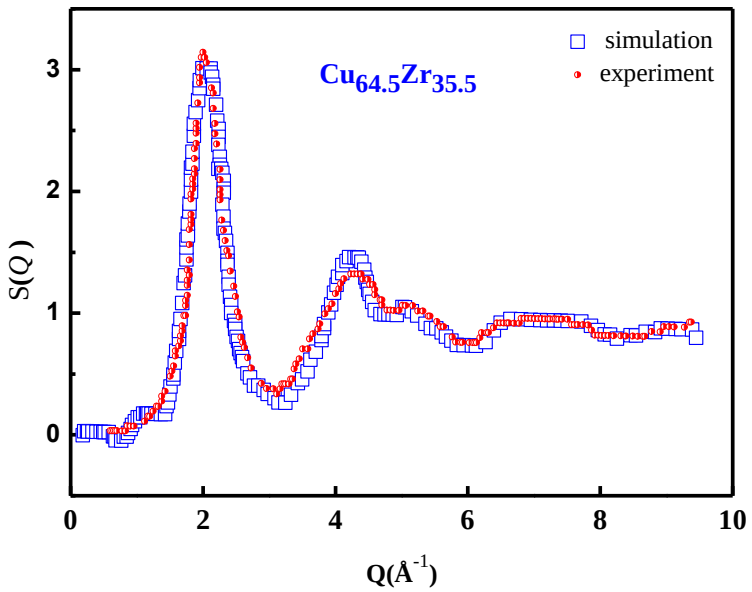

The structure factors $S(q)$ from the simulation $Cu_{64.5}Zr_{35.5}$ sample and experiment.

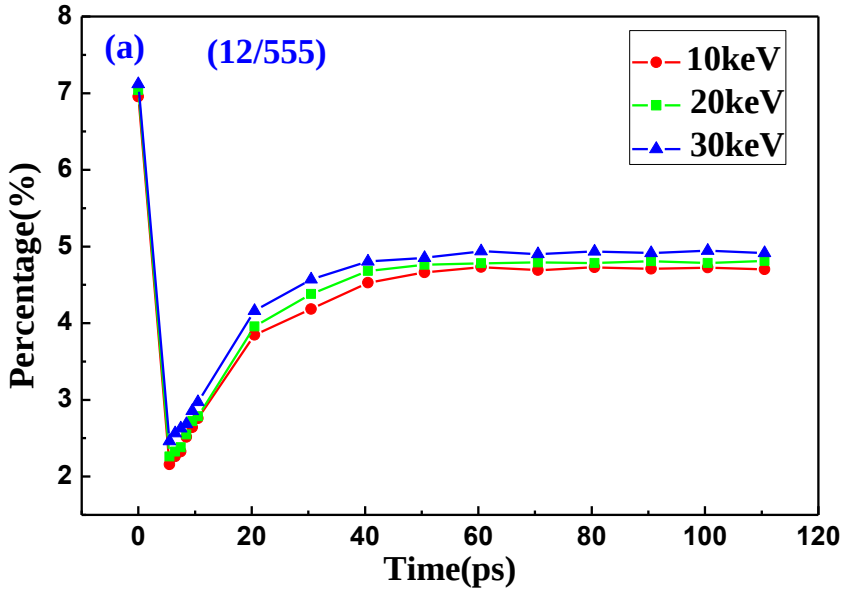

The evolution of FI fraction in the cascade region for PKA energies of 10 keV (red), 20 keV (green), and 30 keV (blue).

The majority of clusters are full and defective icosahedrons,and most of these radiation damages have been self-recovered quickly.

Lang L, Tian Z, Hu W, et al. Molecular dynamics simulations of the structure evolutions of Cu-Zr metallic glasses under. Nuclear Instruments and Methods in Physics Research Section B: Beam Interactions with Materials and Atoms, 2017, 393: 77-81.

MD simulation of displacement cascade in amorphous

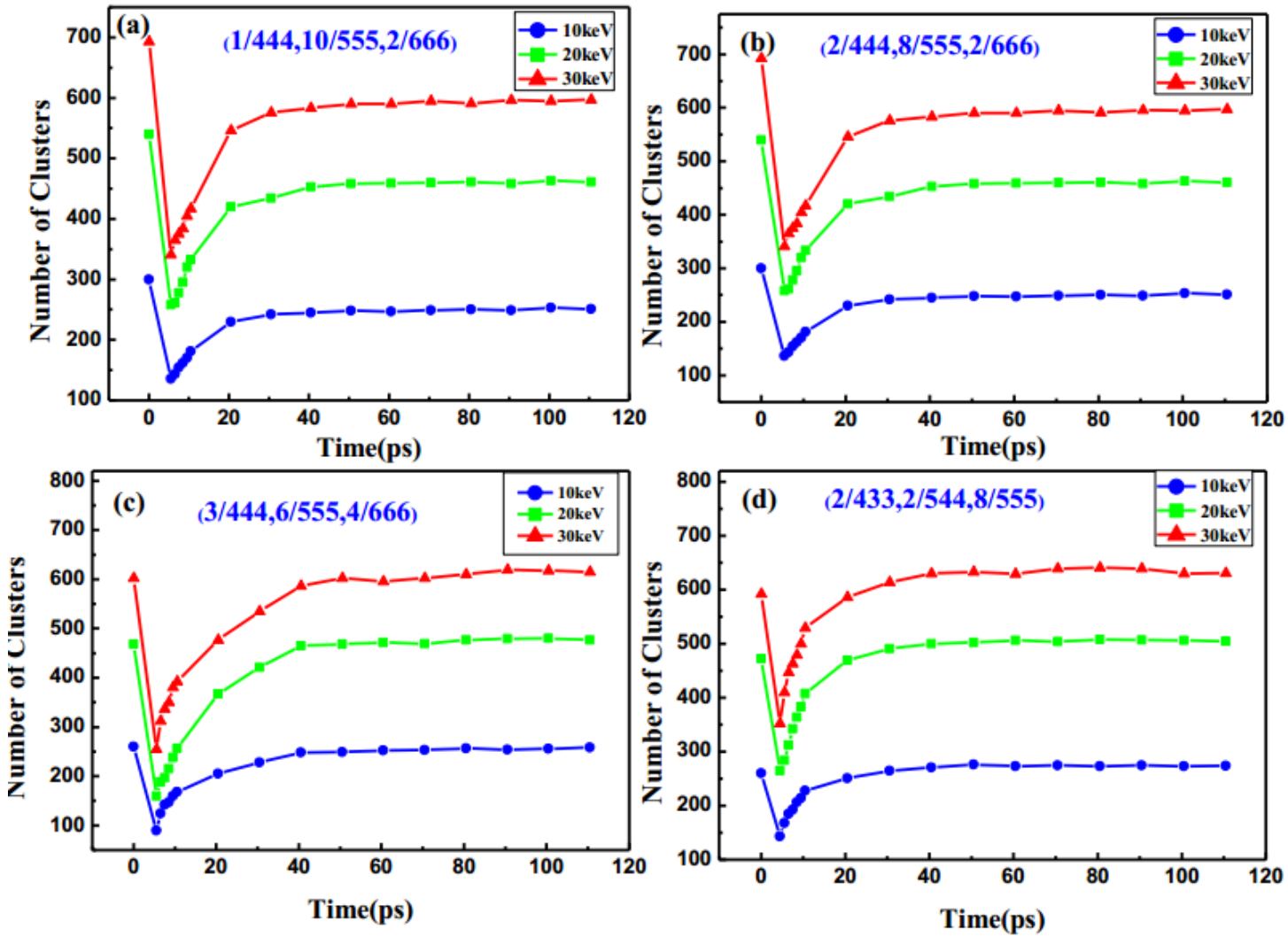

Number evolution of 4 major LSCs in the cascade region for PKA energies of 10keV (red), 20 keV (green), and 30 keV (blue).

MD simulation of displacement cascade in amorphous

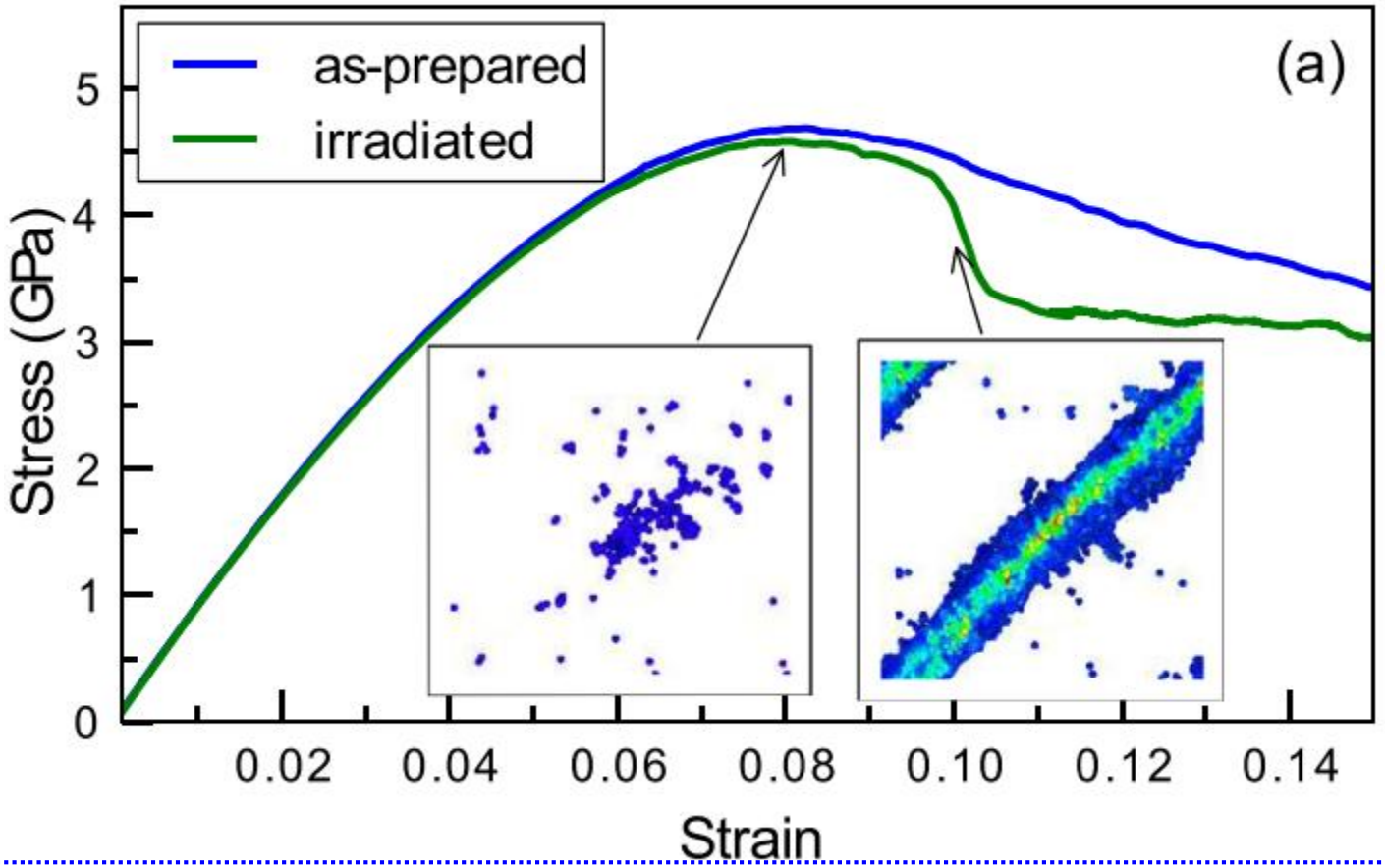

Representative stress-strain curves for tensile deformation of irradiated and as-prepared samples. Inset: left before stress release (strain =0.08) and right after the release (strain =0.10)

Models & Paramters

Table: The model parameters of Fe and Li blocks used to construct the Fe(001) surface and Fe(001)-Li solid-liquid interface samples

	x	y	Z	Lx(Å)	Ly(Å)	Lz(Å)	Atom numbers
Fe	[100]	[010]	[001]	$70a_{Fe}$	$70a_{Fe}$	$80a_{Fe}$	784000
Li	[100]	[010]	[001]	$58a_1$	$58a_2$	$40a_{Li}$	269120

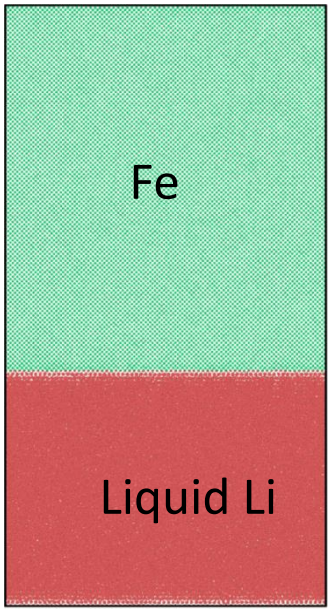

The as-constructed Fe(001)-Li solid-liquid interface sample at 500K

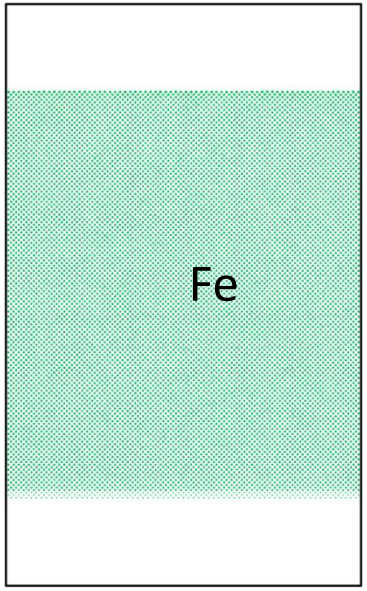

The as-constructed Fe(001) surface sample at 500K

Models & Paramters

PKA: Fe atom E_{PKA}: 20keV

Table: The distances between the PKA and the Fe(001) surface/Fe(001)-Li solid-liquid interface in different samples (PKA is in the vacuum or liquid side)

	The distance from PKA to surface（Å）	The distance from PKA to interface（Å）		
	group 1	group 1	group 2	group 3
sample 1	0	1.54	3.38	8.32
sample 2	0	0.32	4.19	8.83
sample 3	0	0.16	4.56	9.30
sample 4	0	1.62	3.23	7.72
sample 5	0	0.36	4.20	9.00
sample 6	0	1.55	3.18	8.14
sample 7	0	0.16	4.69	9.66
sample 8	0	-0.07	4.85	9.69
sample 9	0	0.14	4.86	9.88
average	0	0.64	4.13	8.95

Morphology Evolution

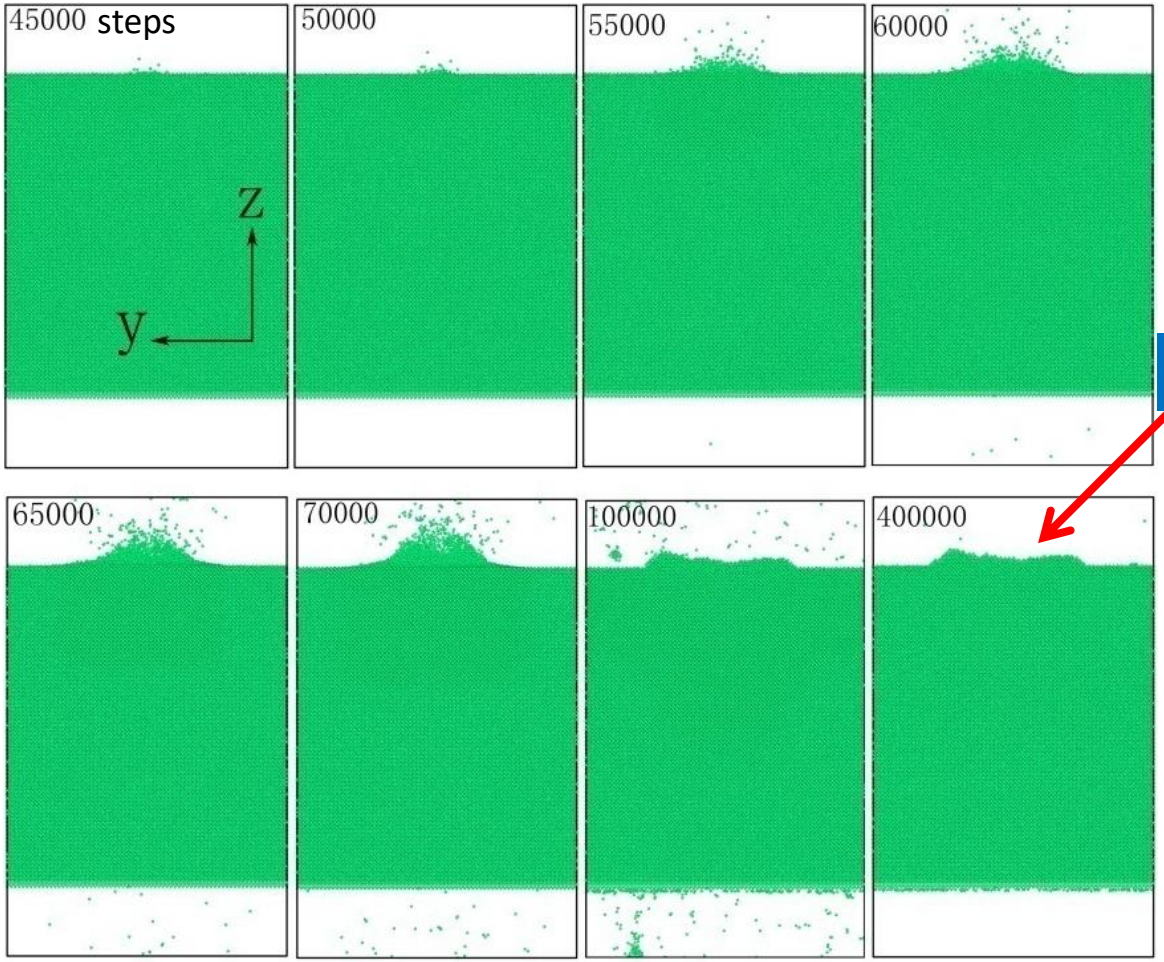

The evolution process of the Fe(001) surface under irradiation at 500K, the distance from the PKA to the surface is equal to 0Å.

Morphology Evolution

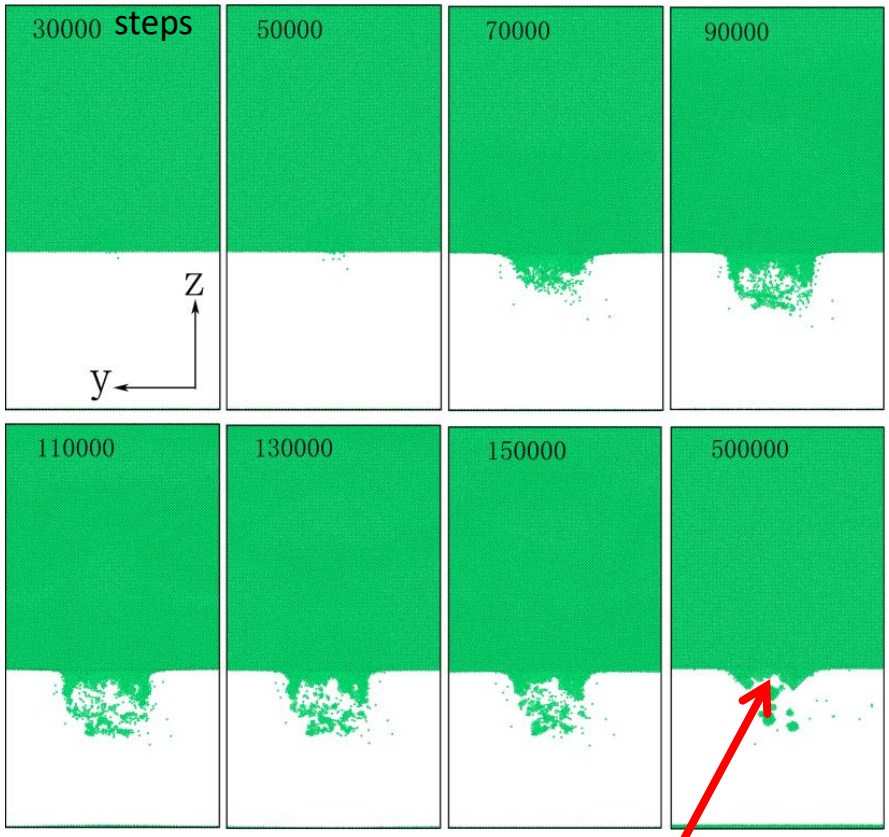

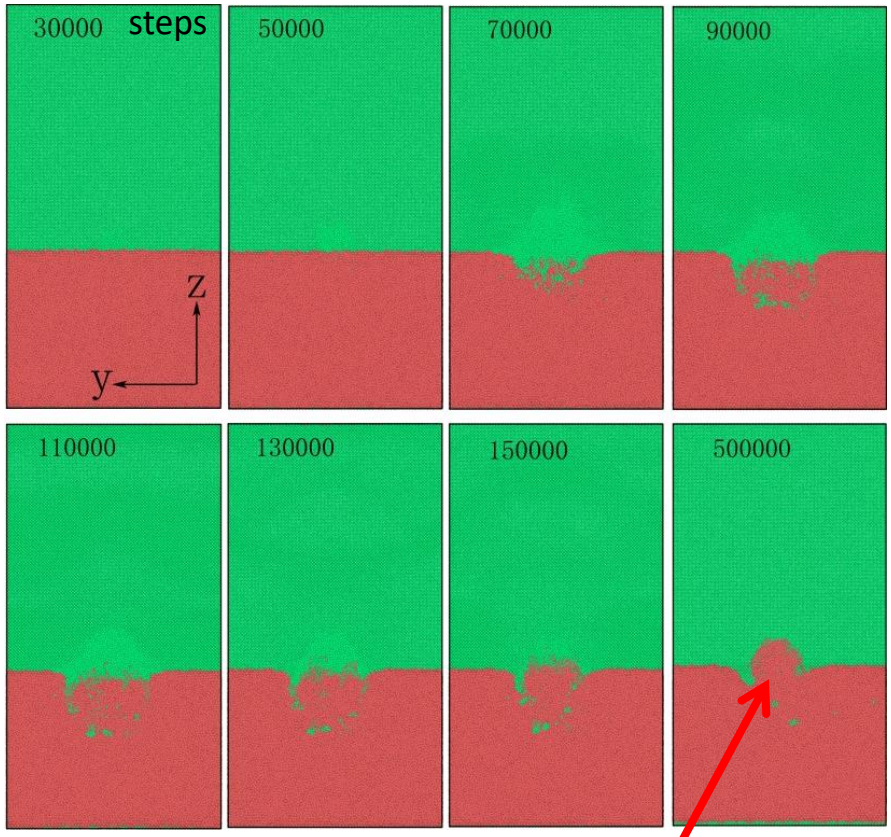

Some atoms are sputtered out and a crater is formed

The crater is filled with liquid Li, but few Li atoms diffuse into the Fe block

The evolution process of the Fe(001)-Li solid-liquid interface under irradiation at 500K, the distance from the PKA to the interface is equal to 0.32Å, in the left one Li atoms are not shown, the right one is a cross-section view.

Morphology Evolution

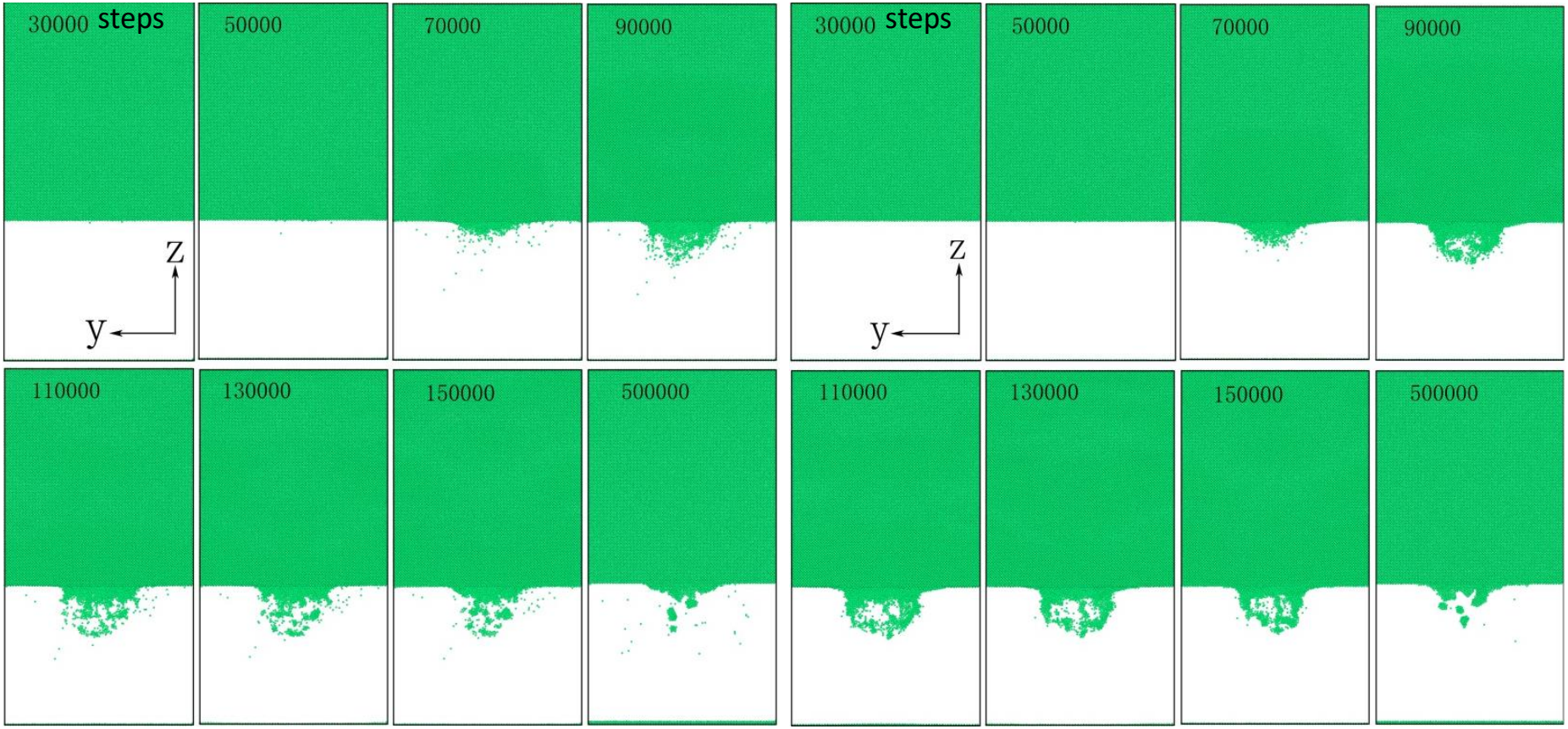

The evolution process of the Fe(001)-Li solid-liquid interface under irradiation at 500K, the distances from the PKA to the interface are equal to 4.13Å (left) and 8.95Å (right) respectively (Li atoms are not shown).

Defects Evolution

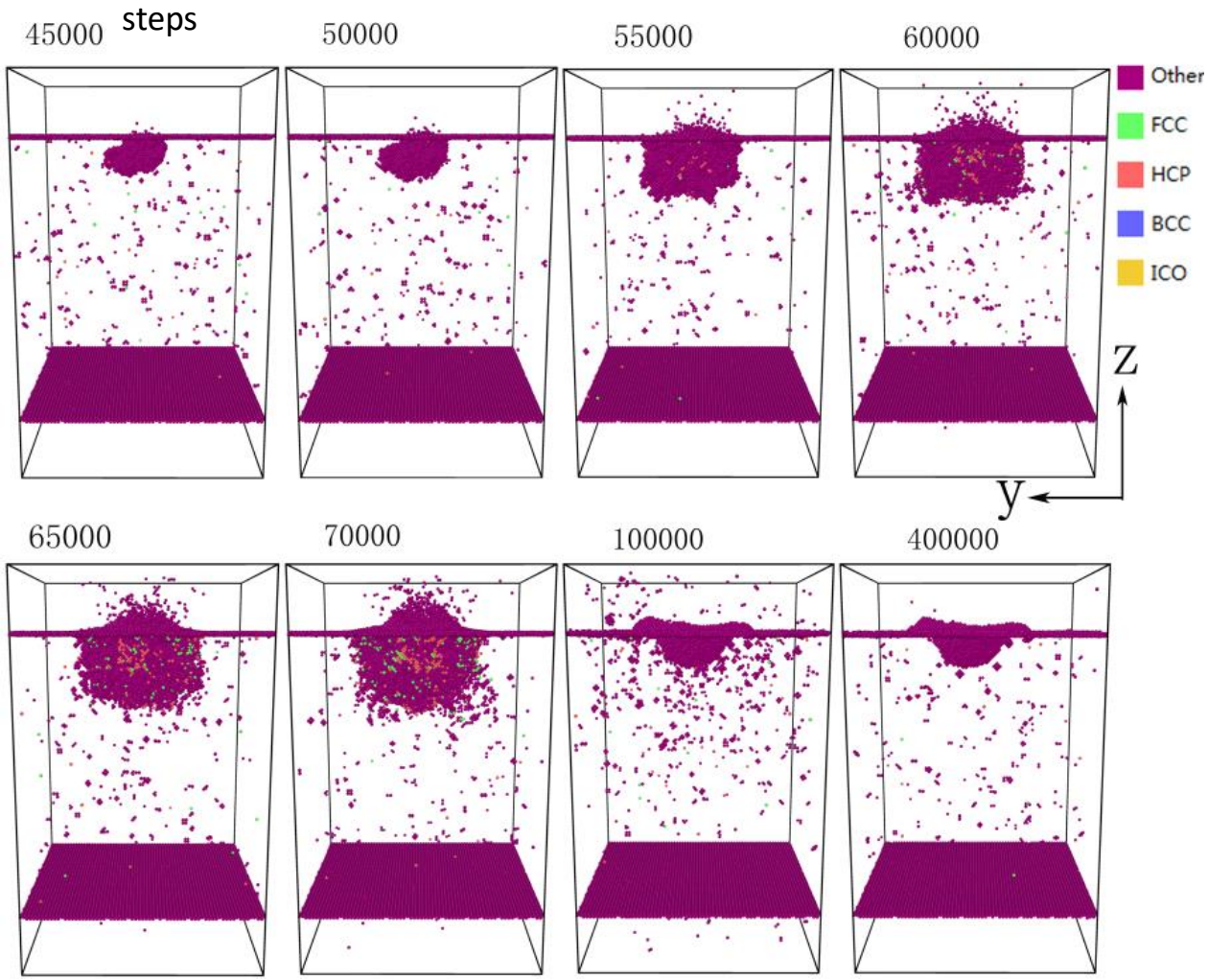

The evolution process of the defect atoms in the Fe(001) surface sample under irradiation at 500K, the distance from the PKA to the surface is equal to 0Å

Defects Evolution

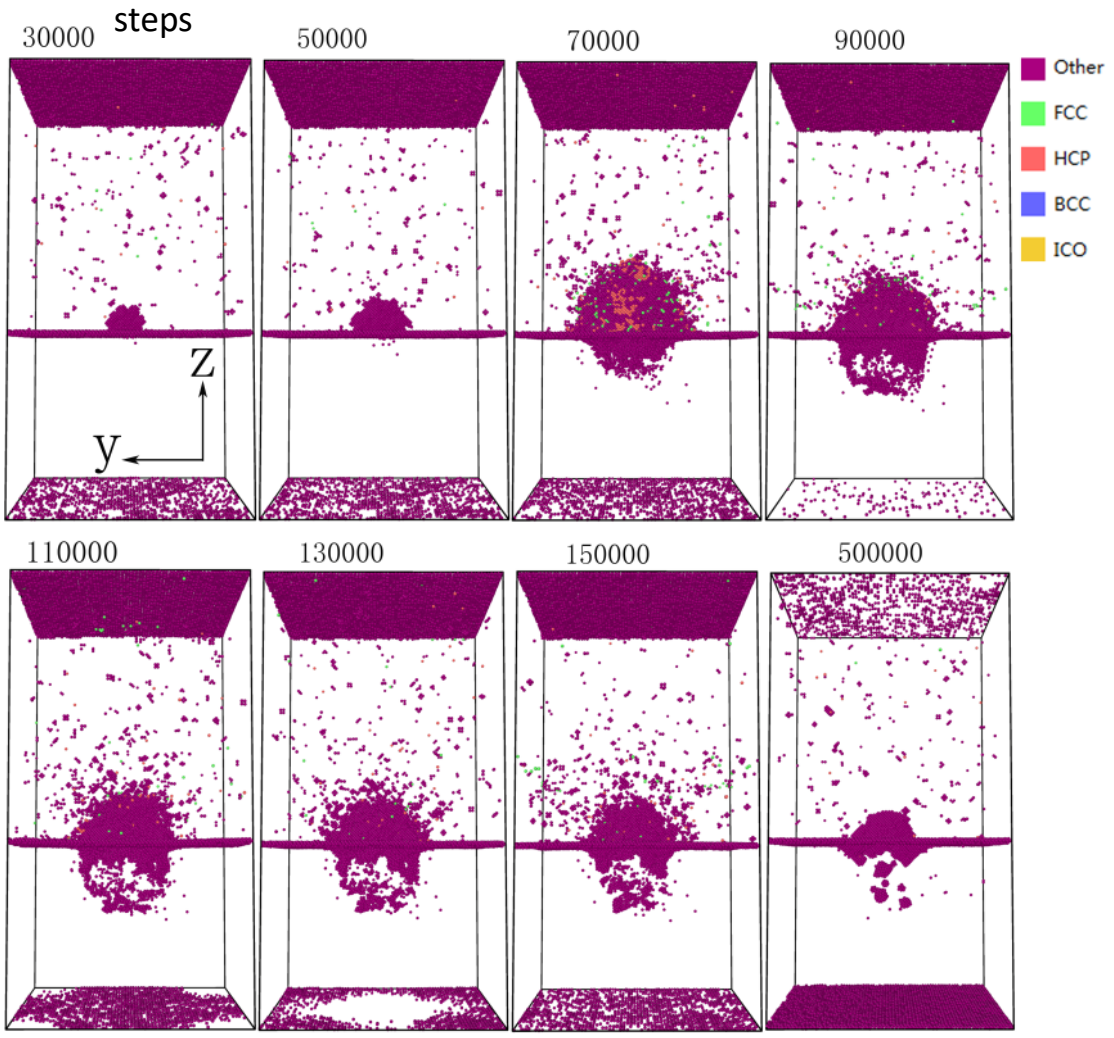

The evolution process of the defect atoms in the Fe(001)-Li solid-liquid interface sample under irradiation at 500K, the distance from the PKA to the interface is equal to 0.32Å

Defects Evolution

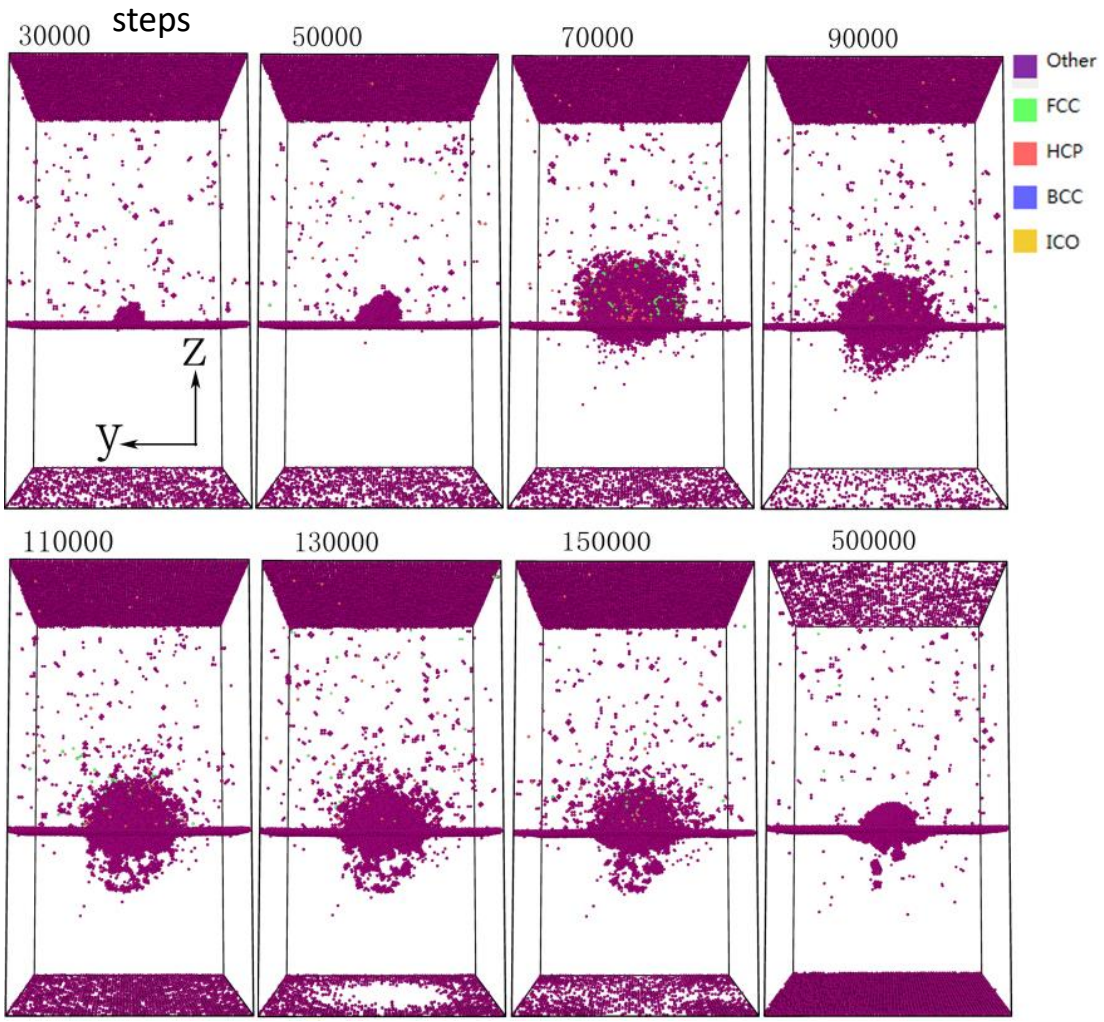

The evolution process of the defect atoms in the Fe(001)-Li solid-liquid interface sample under irradiation at 500K, the distance from the PKA to the interface is equal to 4.13Å

Defects Evolution

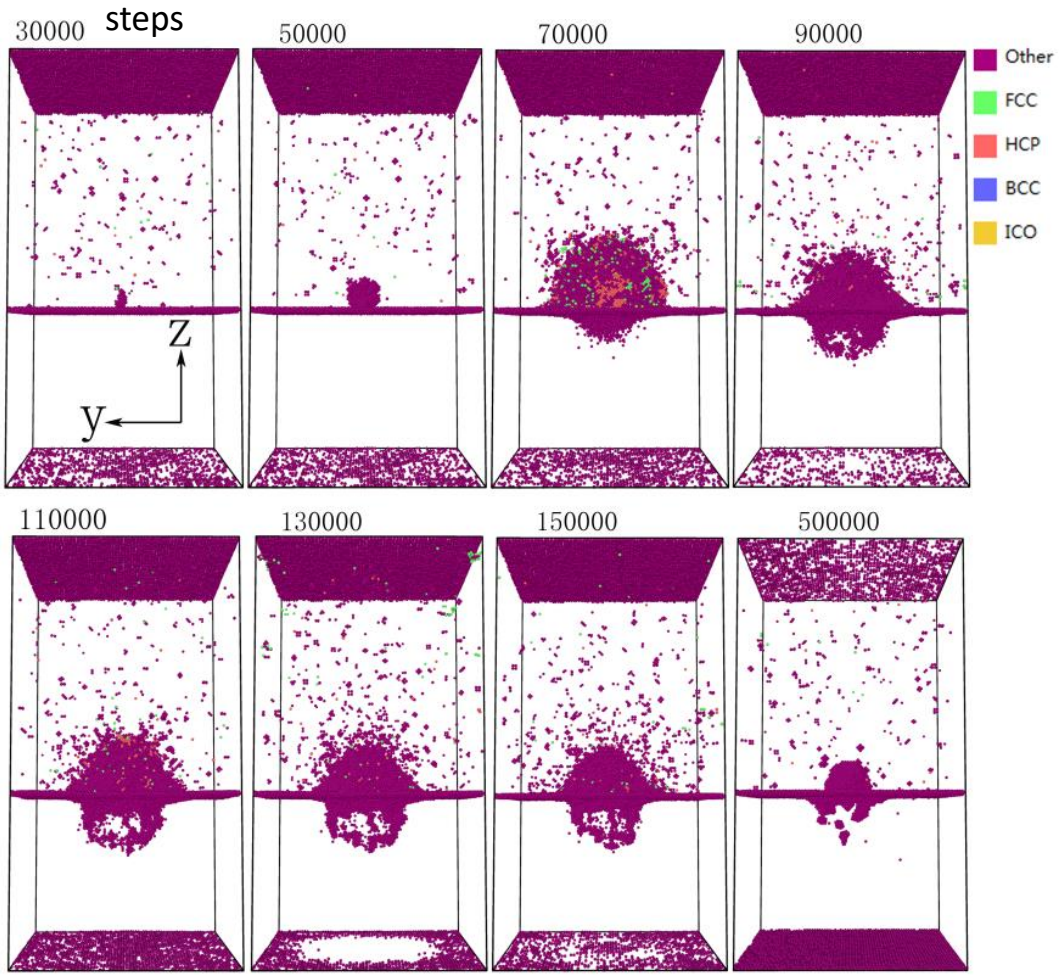

The evolution process of the defect atoms in the Fe(001)-Li solid-liquid interface sample under irradiation at 500K, the distance from the PKA to the interface is equal to 8.95Å

Defects Evolution

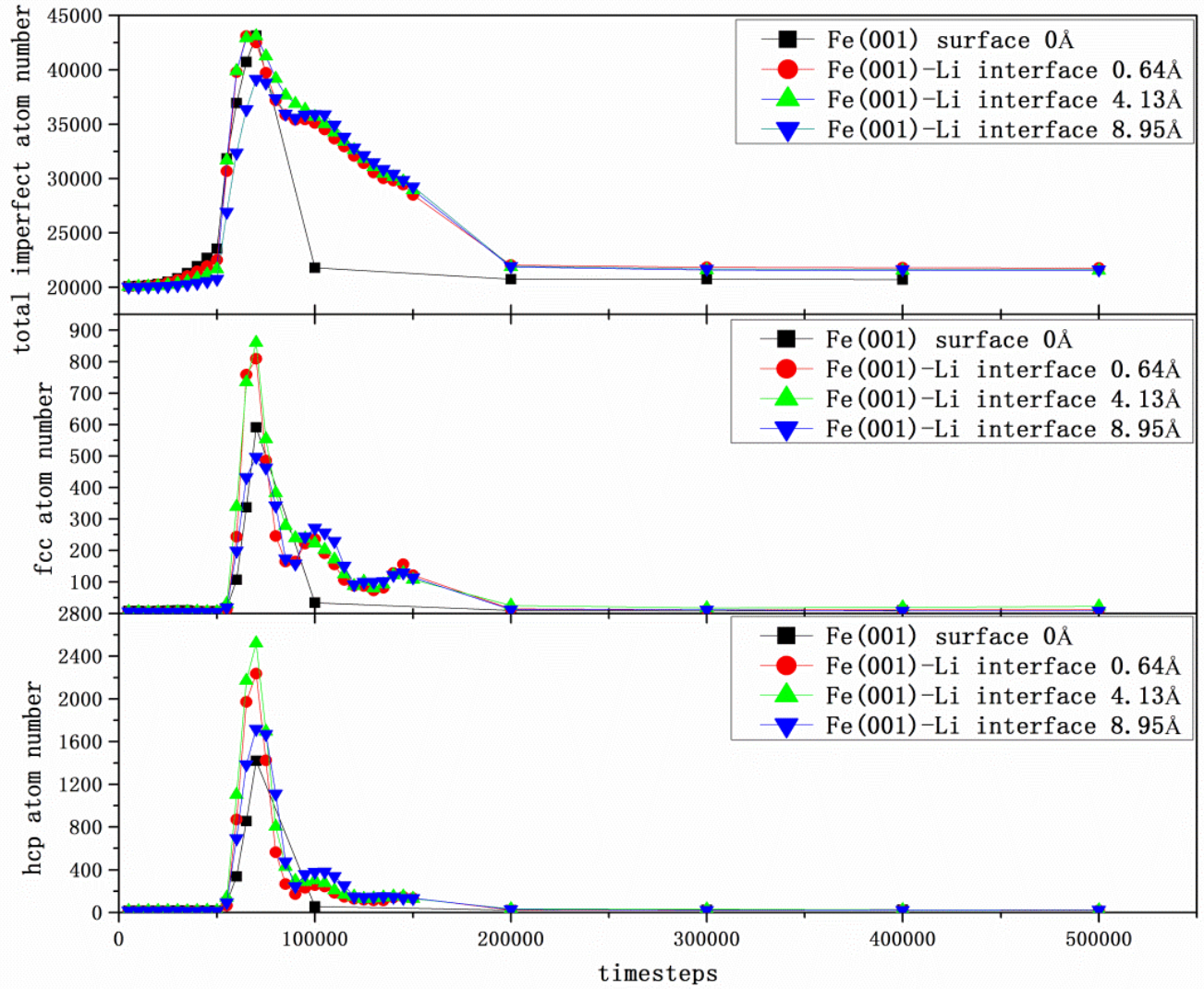

The time step dependence of the average total number of defects, average FCC atoms and HCP atoms at 500K

The existence of liquid Li is beneficial for the sputtered Fe atoms' clustering

Damage Evaluation

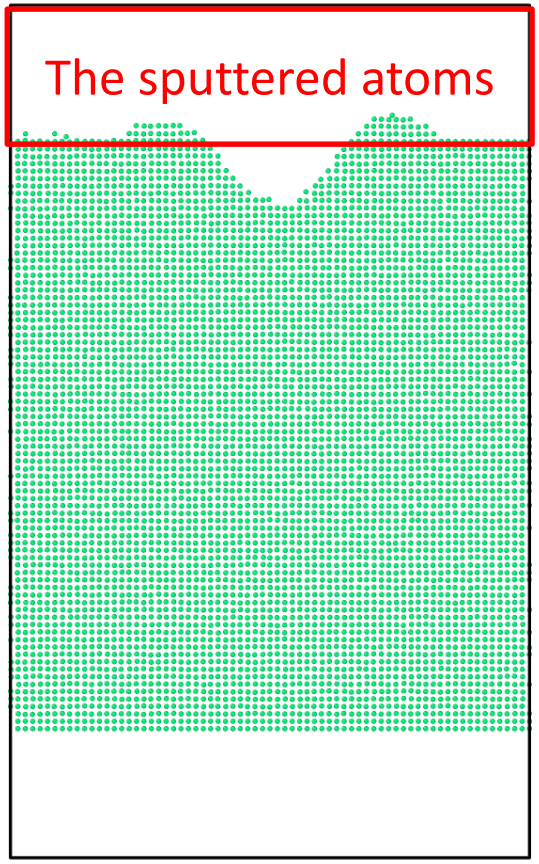

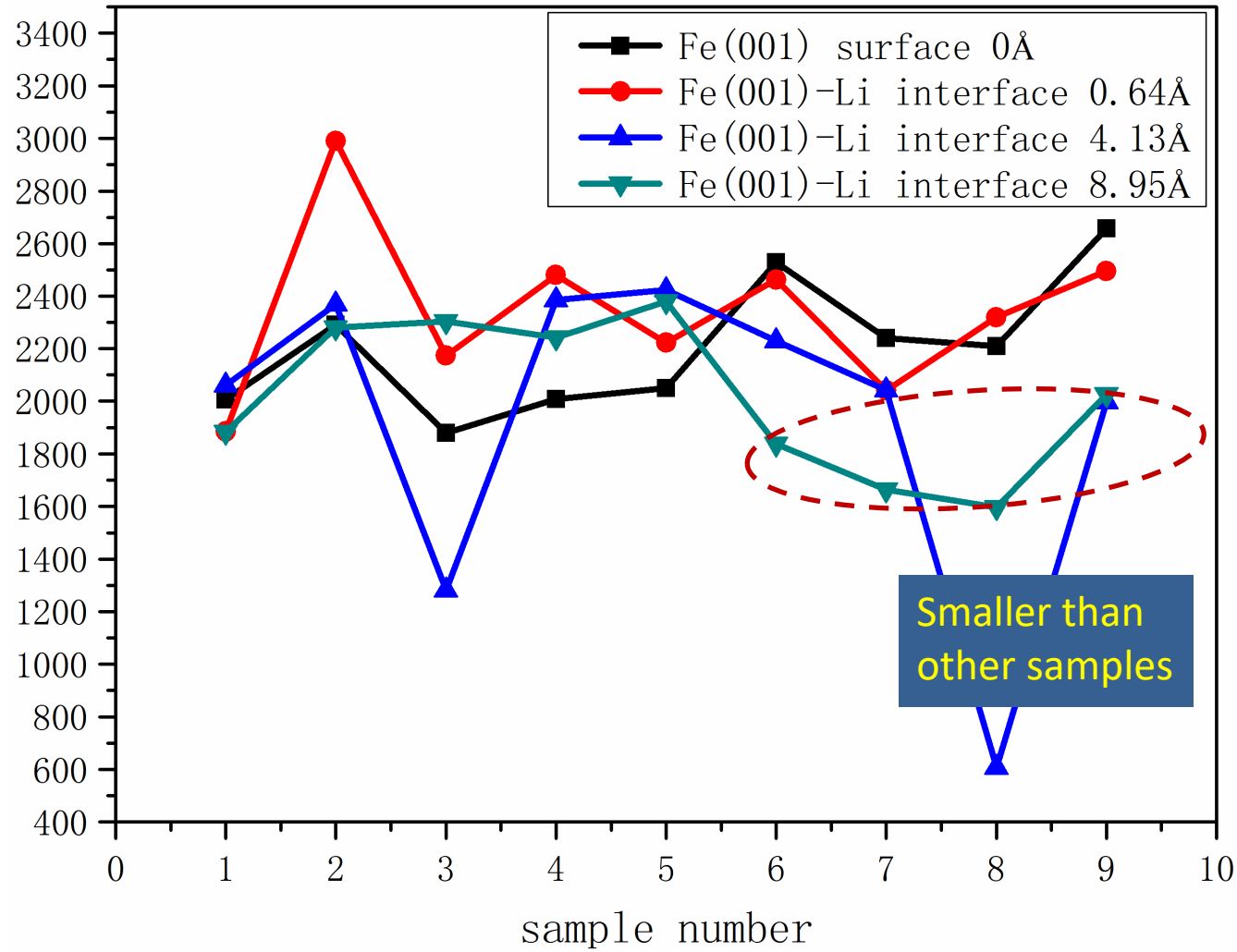

The number of sputtered atoms in each sample

A 4.13 to 8.95Å thick liquid Li layer can partly weaken the damage, caused by the high energy Fe atom after passing through the liquid Li layer, to the Fe block.

Damage Evaluation

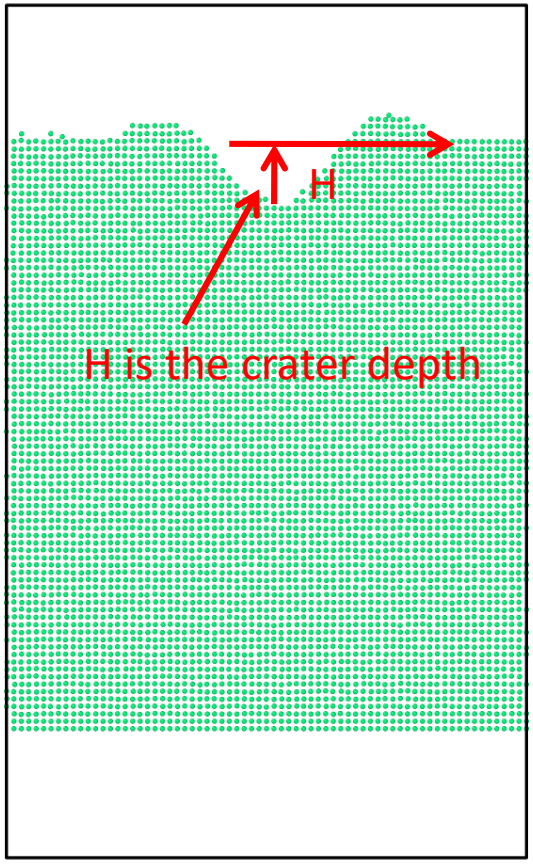

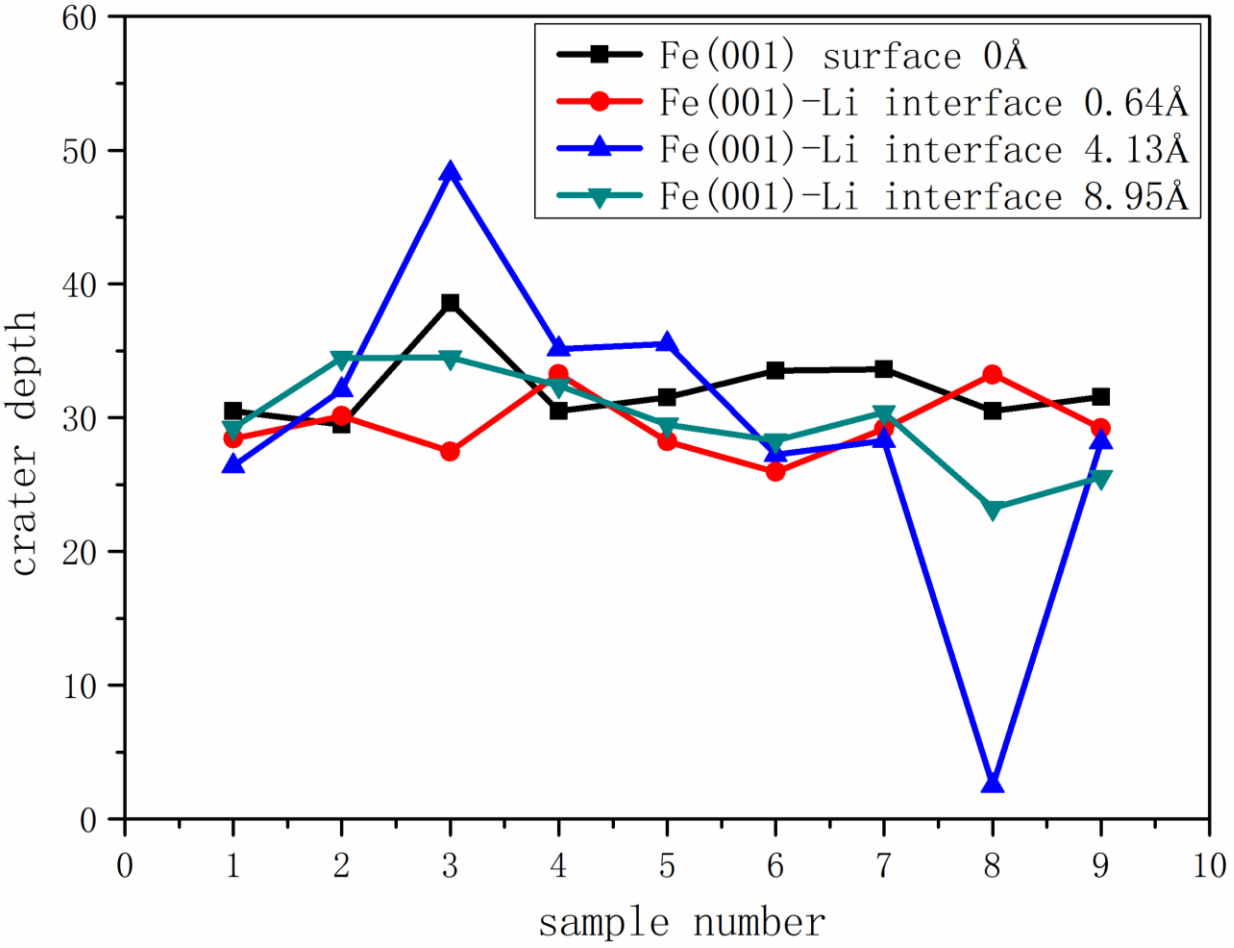

The crater depth in each sample

Thank you for attention! !